RESEARCH METHODS VOLCANICA

VolFe: an open-source Python package for calculating melt-vapour equilibria including silicate melt, carbon, hydrogen, sulfur, and noble gases

Ery C. Hughes*[†α,β], Philippa Liggins[γ], Penny E. Wieser[δ], and Edward M. Stolper[β]

[α]Te Pū Ao GNS Science, National Isotope Centre/Avalon, Lower Hutt 5010, Aotearoa New Zealand.
[β]Division of Geological and Planetary Sciences, Caltech, Pasadena, CA 91125, USA.
[γ]Oxford Research Software Engineering Group, University of Oxford, 1–4 Keble Road, Oxford OX1 3NP, UK.
[δ]Earth and Planetary Science, UC Berkeley, Berkeley, CA, USA.

Abstract

VolFe is an open-source flexible and adaptable thermodynamic framework in Python for calculating the equilibrium composition of melt and vapour. VolFe considers basaltic through rhyolitic melts including the volatiles carbon, hydrogen, sulfur, and the noble gases. VolFe models both reduced and oxidised systems due to the range of melt and vapour species included. Hence, VolFe is applicable to terrestrial (e.g. mid-ocean ridges to arcs) and extra-terrestrial (e.g. the Moon and Mars) systems. New parameterisations of "model-dependent variables" (e.g. volatile solubility functions, sulfide-saturation conditions, fugacity coefficients, etc.) can be added as new experimental studies come out, enhancing VolFe's future applicability. The main calculations currently included in VolFe are the pressure of vapour-saturation based on the dissolved volatile content of melts; H_2O-CO_2 isobars, open- and closed-system degassing and regassing; an oxybarometer based on the melt sulfur content; and uncertainty propagation of the input melt compositions on calculation outputs. As an example, we apply VolFe to melt inclusion and submarine pillow glass data from the Marianas arc.

Keywords: Volatiles; Thermodynamic; Degassing; Open-source; Melt; Vapour.

Submitted: 2024-09-25 | Accepted: 2025-07-16 | Published: 2025-11-03

Editor: K. Iacovino | Typesetter: J. Farquharson

1 Introduction

The behaviour of volatile elements such as carbon (C), hydrogen (H), sulfur (S), the noble gases (He, Ar, Ne, etc.), and the halogens (Cl, Br, etc.) during magmatic and volcanic processes is important in volcanology and igneous petrology. Exsolving vapour from degassing can provide a driving force for eruptions, leading to explosive or quiescent addition of volatiles to the atmosphere that can impact climate and/or human health [e.g. Stewart et al. 2021; Marshall et al. 2022]. Surrounding country rocks can be altered by an exsolved fluid phase, sometimes playing a role in ore formation [e.g. Simon and Ripley 2011]. The loss of volatiles to vapour can also affect the physical properties, chemical compositions, and liquid lines of descent of magmas [e.g. Dingwell et al. 1996; Applegarth et al. 2013]. Additionally, the oxygen fugacity (fO_2) of the system can evolve during degassing because of the differing dominant oxidation states of volatile elements in coexisting melt and vapour [Anderson and Wright 1972; Candela 1986; Carmichael and Ghiorso 1986; Burgisser and Scaillet 2007; Métrich et al. 2009; Gaillard et al. 2011; Kelley and Cottrell 2012; Moussallam et al. 2014; Gaillard et al. 2015; Moussallam et al. 2016; Brounce et al. 2017; Hughes et al. 2023b].

A quantitative understanding of volatile degassing from magmas requires both studies of natural systems and physical and chemical models of degassing to aid in their interpretation [e.g. Papale et al. 2022]. Consequently, there has been considerable interest in developing quantitative models of melt-vapour chemical equilibria for silicate melt-H_2O-CO_2, resulting in a range of applicable tools: e.g. VolatileCalc [Newman and Lowenstern 2002]; MagmaSat [Ghiorso and Gualda 2015]; Solwcad [Papale et al. 2006]; and VESIcal [Iacovino et al. 2021]. More recently, such tools include sulfur: e.g. CHOSETTO [Moretti and Ottonello 2003; Moretti and Papale 2004]; an unnamed tool from Gaillard and others [e.g. Gaillard et al. 2011; Gaillard and Scaillet 2014]; SolEx [Witham et al. 2012]; D-Compress [Burgisser et al. 2015]; EVo [Liggins et al. 2020; 2022]; MAGEC [Sun and Lee 2022; Sun and Yao 2024]; Sulfur_X [Ding et al. 2023]; MELTS+DEW [Ghiorso et al. 2023]; Petrolog4[‡]; and our tool that we now refer to as VolFe [Hughes et al. 2023b; 2024]. Despite differences in their details, these tools typically calculate the equilibrium state of melt-vapour systems given a set of independent variables (e.g. vapour saturation pressures and degassing paths). These tools have been used extensively to interpret natural sample data, such as the compositions of melt inclusions [e.g. Werner et al. 2020; Wieser et al. 2021; Ranta et al. 2024], submarine pillow glasses [e.g. Soule et al. 2012; Brounce et al. 2017; Lund et al. 2018], and volcanic gases [e.g. Aiuppa et al. 2022; Burton et al. 2023].

We note the distinction between individual solubility models for specific volatiles (e.g. equations 1 and 8 for CO_2 or equations 2 and 9 for H_2O solubility in basaltic melts in Dixon [1997])—which we refer to as solubility functions in this paper—and these tools that model systems containing multiple volatiles by combining various solubility models. For instance, VolatileCalc is a tool that includes the CO_2 and H_2O sol-

*ery.hughes@ucl.ac.uk
[†]Now at: Department of Earth Sciences, University College London, 5 Gower Place, London, UK.

[‡]https://petrologsoftware.com/

ubility functions from Dixon [1997] and others. Sometimes a new study will produce both a new solubility function and a new tool: e.g. Ding et al. [2023] describe both a new solubility function for sulfur (their equations 9 and 10 and Table 3) and a new tool called `Sulfur_X` for degassing calculations. Hence, sometimes these tools have their own unique solubility function, other times they incorporate solubility functions already available in the literature, or both.

In this paper we describe `VolFe` and its implementation via an open-source `Python` package for calculating melt-vapour equilibria (available at GitHub* and archived in Zenodo [Hughes et al. 2025]). The name "VolFe" derives from "**Vol**atile + **Fe**" to highlight the role and evolution of fO_2 for processes involving melt-vapour equilibria. Our goal is for `VolFe` to be user-friendly, flexible, adaptable, and to evolve over time as new thermochemical data become available and new applications are envisioned. This tool was initially developed and applied to modeling the sulfur solubility minimum and maximum in silicate melt ± vapour ± sulfide ± anhydrite assemblages for basaltic systems in which the vapour was restricted to S- and O-bearing species only (i.e. no C or H present in the system [Hughes et al. 2023b]) and to examine the influence of sulfur and fO_2 on the pressure of vapour-saturation in magmas (P^v_{sat} [Hughes et al. 2024]). Although the thermodynamic model was fully described in these papers, significant effort has been applied to making the underlying source code more accessible to the community (with the inclusion of documentation and examples), as well as expanding the range of possible calculations that can be performed (e.g. degassing including C, H, and S). The goal of this paper is to explain more fully the structure of the `Python` package and its capabilities, as well as the various assumptions and approximations that are used. To help with implementation by potential users (including those with little or no coding experience), we provide numerous examples of usage through Jupyter Notebooks and fuller documentation via ReadTheDocs†.

2 Thermodynamic framework

We chose a simple thermodynamic approach to construct `VolFe`. The state of the system is calculated by assuming that chemical equilibrium is achieved given the values of the selected independent variables, where paths can be formed by sequential steps of these calculations (e.g. decreasing P would result in degassing). Chemical equilibrium is described by a set of chemical reactions: (1) among species within the melt or vapour phase (i.e. homogeneous equilibria), and (2) between species in the melt and vapour (i.e. heterogeneous equilibria). All these reactions must be linearly independent, meaning none of these reactions can be created by adding or subtracting combinations of the other reactions. Each chemical reaction has an equilibrium constant that constrains the relative concentrations of the reactants and products at equilibrium given the independent variables.

To use this approach, we first choose the phases that might be present and the species within them. Then we choose a set of linearly independent equilibria that relate the species within and between the different phases. We refer to this as the thermodynamic framework of the system (Section 3). The number of independent equilibria (E) required to describe the system is determined by:

$$E = N - c, \tag{1}$$

where N is the total number of species in the system (e.g. the total number of species in the melt and vapour phases) and c is the number of components required to describe possible variations in the composition of the whole system regardless of the actual speciation [e.g. Prigogine and Defay 1954] (Section 3.1). This framework is only as good as its inventory of potential phases, species, and chemical reactions (i.e. thermochemical parameters). Thus, if there are key melt or vapour species in the system of interest to a particular problem that are currently not included in `VolFe` (e.g. the halogens), the results from `VolFe` will not be appropriate. However, the inclusion of oxidised *and* reduced species (e.g. H_2O and H_2; CO_2 and CO, etc.: Section 3) in the melt and vapour means magmas over a wide range of fO_2 can be modelled: from reduced lunar or martian basalts to oxidised arc basalts. Additionally, various combinations of volatiles allow different systems to be modelled, from terrestrial magmas with CHOS-bearing volatiles to magmas on Io with only SO-bearing volatiles.

The values of the thermochemical parameters embedded in `VolFe` depend on the parameterisation chosen to evaluate them at a given set of conditions, which we term "model-dependent variables" (Section 3). These variables include equilibrium constants, solubility functions, fugacity coefficients, definitions of fO_2 buffers, etc. They are termed "model-dependent" because different parameterisations to calculate these variables are available in the literature. For instance, the absolute fO_2 value of the Fayalite-Magnetite-Quartz (FMQ) buffer at a certain P and temperature (T) can be calculated using the parameterisation of Frost [1991] or O'Neill [1987], etc. Hence, the FMQ buffer is a model-dependent variable. Similarly, different parameterisations for the solubility functions of H_2O, CO_2, etc. in volatile-bearing melts [e.g. Dixon et al. 1995; Dixon 1997; Iacono-Marziano et al. 2012; Ghiorso and Gualda 2015] and of the fugacity coefficients for species in the vapour phase [e.g. Holloway 1977; Holland and Powell 1991; Belonoshko and Saxena 1992; Shi and Saxena 1992] exist in the literature. In `VolFe`, we have included various parameterisations from the literature of these model-dependent variables that can be chosen by the user when running calculations, and new ones can be added as desired. For example, if the parameterisations of the solubility function for H_2 currently available in `VolFe` (Supplementary Material Table S8) are not appropriate for a user's system of interest (e.g. either because of new data or to account for their variability as a function of the major element composition of the melt), a new parameterisation could be added (see example in the ReadTheDocs). Where possible, the functions currently available in `VolFe` to calculate these parameterisations have been benchmarked against the original publication (e.g. results described in the text, figures, or tables in the original paper; supplemental calculators provided as supporting spreadsheets; or other codes). The worked calculations to produce

*https://github.com/eryhughes/VolFe
†https://VolFe.readthedocs.io/en/latest/

the benchmarking results are included as Jupyter Notebooks in the GitHub repository and ReadTheDocs and highlighted in Supplementary Material Tables S1–11. The goal is to make `VolFe` adaptable as new parameterisations become available, especially as new experiments are conducted.

Finally, to calculate the state of the system at equilibrium either statically or along a particular path, we require the choice of a set of independent variables whose values we specify for the calculation or at each step along the path. If the relative proportions of the phases are not required (e.g. at P^v_{sat} [Hughes et al. 2024]), the phase rule dictates the number of independent intensive variables (i.e. the variance, F) required to specify the state of the system for a given number of phases (φ) and components [Gibbs 1876; 1878]:

$$F = c + 2 - \varphi. \tag{2}$$

Alternatively, if the equilibrium proportions of the phases are required (e.g. for modelling degassing) we use Duhem's theorem. This states that for a closed-system (i.e. where the masses of all components remain constant and are known), the equilibrium state is completely determined once the values of any two independent intensive and/or extensive variables are specified [e.g. Prigogine and Defay 1954; Powell et al. 1998]. The constancy of the bulk composition of the system to apply Duhem's theorem requires mass balancing all components across all phases present in each step on any specified path (Section 3.3).

Whether the phase rule or Duhem's theorem is the basis for the number and nature of the chosen independent variables, different choices of these variables enable different types of calculations. `VolFe` contains functions to calculate the state of the system at equilibrium given several choices of independent variables (Section 4). These include the pressure of vapour-saturation for a given volatile-bearing melt composition and T (P^v_{sat}, Section 4.1); CO_2–H_2O isobars for a given volatile-free melt composition and T (Section 4.2); the composition of melt and vapour during closed- and open-system degassing or regassing (Section 4.3); and estimating fO_2 from the sulfur content in the melt (Section 4.4). For calculations currently available in `VolFe`, T is always an independent variable and paths are currently isothermal. Alternative choices of the independent variables defining a calculation can be added according to the problem to be solved, allowing flexibility.

3 Phases, species, chemical reactions, and model-dependent variables

The implementation of `VolFe` given here is essentially that described in Hughes et al. [2024] with a few updates (Figure 1). We outline currently available parameterisations of model-dependent variables (e.g. equilibrium constants, fugacity coefficients, etc.) in `VolFe` (Supplementary Material Tables S1–10); interested readers should check the ReadTheDocs for the most up-to-date list. The specific parameterisation for each model-dependent variable can be chosen by the user when running calculations in `VolFe`.

`VolFe` is primarily focused on the two-phase coexistence of melt and vapour (i.e. $\varphi = 2$). We use the term vapour throughout to describe the lower density fluid that may coexist with silicate melt, although super-critical fluid is more appropriate under certain conditions. `VolFe` can also test for saturation with sulfide melt, anhydrite, and/or graphite (see Section 3.4 for further details), but crystallisation of silicate or oxide minerals is not currently considered. The bulk composition of systems currently included in `VolFe` comprise three to six components ($3 < c < 6$): (1) a silicate component, which is defined by the volatile-free composition of the silicate melt and includes all iron as FeO (FeO_T) and all other non-volatile oxides: SiO_2, Al_2O_3, TiO_2, MnO, MgO, CaO, Na_2O, K_2O, and P_2O_5 [e.g. Hughes et al. 2023b; 2024]; (2) the amount of oxygen (O) in excess of the silicate component; and (3–6) at least one of C, H, S, and/or "X". Note that O contained in the silicate component cannot exchange between the melt and vapour. The O that can exchange between the melt and the vapour is contained in the "O in excess of the silicate component": this includes O contained in the vapour; O associated with iron in excess of that already in the silicate component as the silicate component is defined using FeO only; and/or O associated with volatile species in the melt [e.g. Hughes et al. 2023b]. For molecular melt species (i.e. CO, $CO_{2,\text{mol}}$), all O present in the species is counted towards the excess O. For the ionic melt species (CO_3^{2-} and SO_4^{2-}), all but one of the oxygens is counted towards the excess O—the final O is associated with the silicate component (e.g. CaO, Na_2O), which does not exchange between the melt and vapour (i.e. they are treated as CO_2 and SO_3). All O present in H_2O_T is included in the O budget. "X" represents a non-reactive, molecular volatile species—such as a noble gas—and its chemical identity is governed by its molecular mass, fugacity coefficient, and solubility

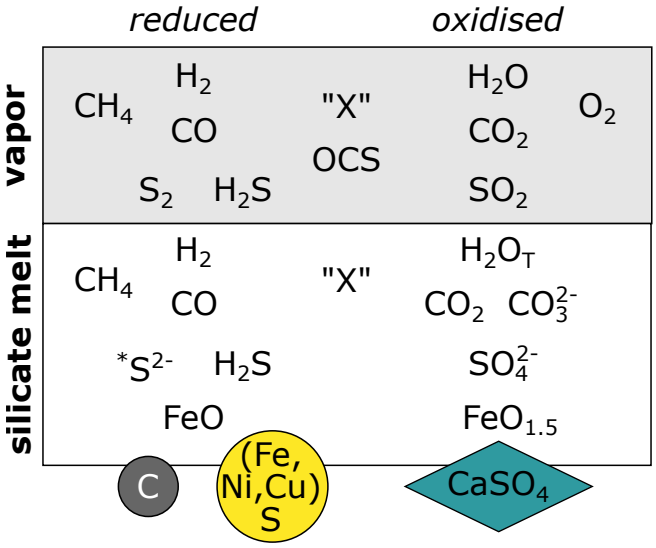

Figure 1: Phases and species considered in the thermodynamic framework of `VolFe`. Generally, reduced species are to the left and oxidised species are to the right. "X" represents a non-reactive molecular volatile species, such as a noble gas. Along the bottom, the small dark-grey circle represents graphite; the large yellow circle liquid sulfide; and the blue diamond anhydrite.

function (described in the sub-sections below). Currently "X" can be either Ar or Ne in VolFe.

The species present in the melt and vapour (Section 3.1 and 3.2) are selected automatically by VolFe based on which volatiles are present in non-zero concentrations for the user-specified composition. Certain melt and vapour species can be excluded if required: e.g. treating H_2, CO, CH_4, and/or H_2S as completely insoluble in the melt or assuming these species are not present in the vapour. There are some limitations on the combinations of species possible (e.g. currently, the re/degassing calculation, cannot have both S and "X" present in the bulk composition).

3.1 Vapour

The vapour has a bulk composition described by five components (C, O, H, S, and "X") and currently includes 11 chemical species (Figure 1): O_2, H_2, CO, S_2, H_2O, CO_2, SO_2, CH_4, OCS, H_2S, and "X". These vapour species are related through six, linearly independent, homogeneous vapour equilibria (Equations 3–8, Table 1). Each homogenous vapour reaction has an equilibrium constant (K) that depends only on T. Although others could be added, currently only a single parameterisation for each K is available in VolFe from Moussallam et al. [2019], O'Neill and Mavrogenes [2022], and Ohmoto and Kerrick [1977], which have been benchmarked where possible (further details are available in Supplementary Material Table S1, with worked calculations available as Jupyter Notebooks on the GitHub repository and ReadTheDocs).

Table 1: Homogeneous vapour equilibria considered in VolFe.

Reaction among vapour species	Equilibrium constant ($K_{X(Y)}$)	
$H_2 + 0.5O_2 \rightleftharpoons H_2O$	$K_H(T) = \frac{f_{H_2O}}{f_{H_2} f_{O_2}^{0.5}}$	(3)
$CO + 0.5O_2 \rightleftharpoons CO_2$	$K_C(T) = \frac{f_{CO_2}}{f_{CO} f_{O_2}^{0.5}}$	(4)
$0.5S_2 + O_2 \rightleftharpoons SO_2$	$K_S(T) = \frac{f_{SO_2}}{f_{S_2}^{0.5} f_{O_2}}$	(5)
$CH_4 + 2O_2 \rightleftharpoons CO_2 + 2H_2O$	$K_{CH}(T) = \frac{f_{CO_2} f_{H_2O}^2}{f_{CH_4} f_{O_2}^2}$	(6)
$0.5S_2 + H_2O \rightleftharpoons H_2S + 0.5O_2$	$K_{HS}(T) = \frac{f_{H_2S} f_{O_2}^{0.5}}{f_{S_2}^{0.5} f_{H_2O}}$	(7)
$OCS + 2CO_2 \rightleftharpoons 3CO + SO_2$	$K_{SC}(T) = \frac{f_{CO}^3 f_{SO_2}}{f_{CO_2}^2 f_{OCS}}$	(8)

$K_{X(Y)}(T)$ is the equilibrium constant involving component X and additionally Y where relevant (oxygen is always involved and therefore not indicated: e.g. K_{SC} is for S- and C-bearing vapour species) and f_i is the fugacity of species i.

The partial pressure (p_i), mole fraction (x_i^v), and fugacity (f_i) for each vapour species (i) are related by:

$$p_i = \frac{f_i}{\gamma^v} = x_i^v P, \tag{9}$$

(Equation 3.20 in Denbigh [1981]), where γ_i^v is the fugacity coefficient. We treat the vapour as an ideal mixture of non-ideal gases (i.e. the Lewis-Randall rule; Equation 3.72 in Denbigh [1981]) such that the γ_i^v of each vapour species depends on P and T but not on the vapour composition. This is a common simplification used in many melt-vapour equilibria tools (e.g. VolatileCalc, D-Compress, Sulfur_X, MAGEC, etc.) and given current uncertainties, the added complexity of modelling a non-ideal mixture of non-ideal gases does not seem necessary [Iacovino 2015]. Currently available parameterisations in VolFe of γ_i^v are from Shaw and Wones [1964], Shi and Saxena [1992] (including modifications described in Hughes et al. [2023b, 2024]), Holland and Powell [1991], and the Flowers [1979] correction to Holloway [1977] modified from MIMiC [Rasmussen et al. 2020] and originally from VolatileCalc [Newman and Lowenstern 2002]; which have been benchmarked where possible (Supplementary Material Table S2 and associated Jupyter Notebooks on the GitHub repository and ReadTheDocs). Additionally, VolFe can treat any vapour species as ideal (i.e. $\gamma_i^v = 1$). At equilibrium, the sum of the partial pressures of all the vapour species equals the total pressure of the system (Equation 3.21 in Denbigh [1981]):

$$P = \sum_{i=1}^{n} p_i = P_{sat}^v. \tag{10}$$

3.2 Volatile solubility in the melt

The whole system (i.e. melt and vapour) is described by six components: C, O, H, S, "X", plus the volatile-free silicate component in which all Fe is present as FeO. VolFe currently includes ten volatile-bearing chemical species in the melt (Figure 1): molecular H_2 ($H_{2,mol}$), H_2O_T (all oxidised hydrogen: the combination of OH^- and H_2O_{mol}), molecular CO (CO_{mol}), carbonate ions (CO_3^{2-}), molecular CO_2 ($CO_{2,mol}$), molecular CH_4 ($CH_{4,mol}$), sulfide ions other than H_2S ($^*S^{2-}$), sulfate ions (SO_4^{2-}), molecular H_2S (H_2S_{mol}), and an inert molecular element ("X"$_{mol}$). There are two additional, volatile-free silicate melt "species": FeO and $FeO_{1.5}$ (Figure 1). The heterogeneous melt-vapour equilibria describing volatile solubility in the melt are listed in Table 2 and derived in full in the Supplementary Material of Hughes et al. [2024].

Depending on the silicate melt composition, CO_2 can dissolve dominantly as $CO_{2,mol}$ and/or as CO_3^{2-} formed by reaction with the silicate-dominated molecular framework of the melt [e.g. Fine and Stolper 1985; 1986; Brooker et al. 1999; Behrens et al. 2004; Botcharnikov et al. 2006]. However, the total amount of carbon dissolved as oxidised species (i.e. $CO_{2,T} = CO_{2,mol}$ and CO_3^{2-}) in any given melt composition is approximately proportional to fCO_2 regardless of the relative amount of $CO_{2,mol}$ and CO_3^{2-} in the melt (e.g. Stolper et al. [1987]; full derivation in the Supplementary Material of Hughes et al. [2024]). Hence, we have chosen to use a single heterogeneous melt-vapour equilibrium (Equation 14 in Table 2) combined with a homogeneous melt equilibria between $CO_{2,mol}$

Table 2: Heterogeneous melt-vapour equilibria considered in `VolFe`.

Solubility mechanism	Solubility function	
$H_2(v) \rightleftharpoons H_{2,mol}(m)$	$f_{H_2} = \frac{w^m_{H_{2,mol}}}{C_{H_{2,mol}}}$	(11)
$H_2O(v) \rightleftharpoons H_2O_T(m)$	$f_{H_2O} \approx \frac{\left(x^m_{H_2O_T}\right)^2}{C_{H_2O_T}}$	(12)
$CO(v) \rightleftharpoons CO_{mol}(m)$	$f_{CO} = \frac{w^m_{CO_{mol}}}{C_{CO_{mol}}}$	(13)
$CO_2(v) \rightleftharpoons CO_{2,T}(m)$	$f_{CO_2} = \frac{x^m_{CO_{2,T}}}{C_{CO_{2,T}}}$	(14)
$CH_4(v) \rightleftharpoons CH_{4,mol}(m)$	$f_{CH_4} = \frac{w^m_{CH_{4,mol}}}{C_{CH_{4,mol}}}$	(15)
$0.5S_2(v) + O^{2-}(m) \rightleftharpoons {}^*S^{2-}(m) + 0.5O_2(v)$	$f_{S_2} = \left(\frac{w^m_{{}^*S^{2-}}}{C_{{}^*S^{2-}}}\right)^2 f_{O_2}$	(16)
$0.5S_2(v) + 1.5O_2(v) + O^{2-}(m) \rightleftharpoons SO_4^{2-}(m)$	$f_{S_2} = \left(\frac{w^m_{SO_4^{2-}}}{C_{SO_4^{2-}}}\right)^2 f_{O_2}^{-3}$	(17)
$H_2S(v) \rightleftharpoons H_2S_{mol}(m)$	$f_{H_2S} = \frac{w^m_{H_2S_{mol}}}{C_{H_2S_{mol}}}$	(18)
"X"$(v) \rightleftharpoons$ "X"(m)	$f_{\text{"X"}} = \frac{w^m_{\text{"X"}}}{C_{\text{"X"}}}$	(19)

v = vapour; m = melt; mol = molecular; f_i = fugacity of species i; x^m_i = mole fraction or w^m_i = concentration (depending on the units) of species i in the melt; C_i = the solubility function for species i, which is the constant of proportionality between the fugacity(ies) and the mole fraction/concentration of species i in the melt; ${}^*S^{2-}$ = sulfide associated with cations in the silicate melt, rather than associated with H, i.e. H_2S_{mol}. The units of the solubility functions for H_2, CO, CH_4, H_2S, and "X" use ppm by weight (ppmw) in the melt for concentration and bars for the fugacity in the vapour. The solubility functions for H_2O_T and $CO_{2,T}$ relate the mole fraction of H_2O_T or $CO_{2,T}$ in the melt (ignoring S and "X") to the fugacity of H_2O or CO_2 in the vapour in bars, respectively: $x^m_i = \left(\frac{w^m_i}{M_i}\right) \Big/ \left(\left[\frac{w^m_{CO_{2,T}}}{M_{CO_2}}\right] + \left[\frac{w^m_{H_2O_T}}{M_{H_2O}}\right] + \left[\frac{\left(1 - w^m_{CO_{2,T}} - w^m_{H_2O_T}\right)}{M_m}\right]\right)$, where M_i is the molecular mass of species i and the molecular mass of the melt (M_m) is of the volatile-free silicate melt composition on a single-oxygen basis as described in Dixon et al. [1995].

and CO_3^{2-} to speciate $CO_{2,T}$ in the melt (e.g. Botcharnikov et al. [2006]; Stolper et al. [1987]; Equation 20 in Table 3).

Table 3: Additional equilibria considered in `VolFe`.

Reaction	
$CO_{2,mol}(m) + O^{2-}(m) \rightleftharpoons CO_3^{2-}(m)$	(20)
$FeO(m) + 0.25O_2(v) \rightleftharpoons FeO_{1.5}(m)$	(21)

Water is known to dissolve in silicate melt as both H_2O_{mol} and OH^- [e.g. Burnham and Davis 1974; Mysen et al. 1980; Stolper 1982a; Dixon et al. 1995; Lesne et al. 2011b]. However, as in Hughes et al. [2024], we use Sievert's law as an approximation for the solubility of H_2O in the melt (i.e. Equation 12 in Table 2), which is a convenient and widely-used approximation appropriate up to ~6.4 wt.% H_2O_T [e.g. Burnham 1979; Stolper 1982b; Ghiorso and Gualda 2015].

In many cases, people are interested in sub-systems of the full system illustrated in Figure 1, in which case the number of linearly independent statements of equilibria reduces. For example, suppose the system of interest contained negligible sulfur. Then we could remove all the sulfur-bearing species

and their associated linearly independent equations. This is done automatically in VolFe if the volatile concentration of a particular component is 0.

3.3 Mass balance

When using Duhem's theory (e.g. for degassing calculations), mass must be conserved for all components within the system. Mass balance for each component distributed between melt and vapour is given by [e.g. Burgisser et al. 2015; Liggins et al. 2020]:

$$w_i^T = M_i \left(w_v^T \left[\left(\frac{n_i^v}{m_v^T} \right) - n_i^m \right] + n_i^m \right), \tag{22}$$

where i refers to the i^{th} component (i.e. C, H, S, O, or "X"); w_i^T is the total weight fraction of this component in the system; M_i is the molar mass of i; w_v^T is the weight fraction of vapour in the system; n_i^j is the moles of i in phase j; and m_v^T is the mass of the vapour defined as:

$$\begin{aligned} m_v^T = {} & \\ & M_{O_2} x_{O_2}^v + M_{H_2} x_{H_2}^v + M_{H_2O} x_{H_2O}^v + M_{CO} x_{CO}^v + M_{CO_2} x_{CO_2}^v \\ & + M_{CH_4} x_{CH_4}^v + M_{S_2} x_{S_2}^v + M_{SO_2} x_{SO_2}^v + M_{H_2S} x_{H_2S}^v \\ & + M_{OCS} x_{OCS}^v \end{aligned} \tag{23}$$

For carbon, i = C and in the vapour:

$$n_C^v = x_{CO_2}^v + x_{CO}^v + x_{CH_4}^v + x_{OCS}^v, \tag{24}$$

where x_j^v is the mole fraction of species j in the vapour. In the melt:

$$n_C^m = \frac{w_{CO_{2,T}}^m}{M_{CO_{2,T}}} + \frac{w_{CH_4}^m}{M_{CH_4}} + \frac{w_{CO}^m}{M_{CO}}. \tag{25}$$

For hydrogen, i = H:

$$n_H^v = x_{H_2O}^v + x_{H_2}^v + 2x_{CH_4}^v + x_{H_2S}^v, \tag{26}$$

$$n_H^m = \frac{w_{H_2O_T}^m}{M_{H_2O}} + \frac{w_{H_2}^m}{M_{H_2}} + \frac{2w_{CH_4}^m}{M_{CH_4}} + \frac{w_{H_2S}^m}{M_{H_2S}}. \tag{27}$$

In the case of H, a factor of 2 is applied to the right-hand side of Equation 22 as the component is treated as H_2.

For sulfur, i = S:

$$n_S^v = x_{SO_2}^v + 2x_{S_2}^v + x_{H_2S}^v + x_{OCS}^v, \tag{28}$$

$$n_S^m = \frac{w_{SO_4^{2-}}^m}{M_{SO_4^{2-}}} + \frac{w_{*S^{2-}}^m}{M_{*S^{2-}}} + \frac{w_{H_2S}^m}{M_{H_2S}}. \tag{29}$$

For oxygen i = O, such that:

$$n_O^v = 2x_{O_2}^v + 2x_{CO_2}^v + x_{CO}^v + x_{OCS}^v + x_{H_2O}^v + 2x_{SO_2}^v, \tag{30}$$

$$\begin{aligned} n_O^m = {} & \frac{2w_{CO_{2,T}}^m}{M_{CO_{2,T}}} + \frac{w_{CO}^m}{M_{CO}} + \frac{w_{H_2O_T}^m}{M_{H_2O}} + \frac{3w_{SO_4^{2-}}^m}{M_{SO_4^{2-}}} \\ & + \frac{w_{Fe}^T}{M_{Fe}} \left(\frac{1.5 \left(\frac{Fe^{3+}}{Fe^{2+}} \right) + 1}{\left(\frac{Fe^{3+}}{Fe^{2+}} \right) + 1} \right). \end{aligned} \tag{31}$$

Note that SO_4^{2-} only contributes three oxygen's as the fourth O is part of the silicate component. The Fe-term in Equation 31 is not included in the first n_O^m-term in Equation 22 because Fe is not present in the vapour.

And for species "X", i = "X":

$$n_{\text{"X"}}^v = x_{\text{"X"}}^v, \tag{32}$$

$$n_{\text{"X"}}^m = \frac{w_{\text{"X"}}^m}{M_{\text{"X"}}}. \tag{33}$$

3.4 Solubility functions and their dependence on *P*, *T*, and melt composition

The formulations and parameterisations of the solubility functions in Table 2 as functions of P, T, and melt composition are key to the quantification of melt-vapour equilibria using VolFe. As in Hughes et al. [2024], we use the broad term "solubility function" rather than the thermodynamically rigorous "equilibrium constant".

As an example, we consider the dissolution of S_2 from the vapour into the melt as $^*S^{2-}$ (all sulfide dissolved in the melt apart from H_2S_{mol}) based on the solubility mechanism given in Table 2 as Equation 17. We can write the equilibrium constant for this reaction ($K_{*S^{2-}}$) as:

$$K_{*S^{2-}}(P,T) = a_{*S^{2-}}^m \left(\frac{f_{O_2}}{f_{S_2}} \right)^{0.5} = \gamma_{*S^{2-}}^m w_{*S^{2-}}^m \left(\frac{f_{O_2}}{f_{S_2}} \right)^{0.5}, \tag{34}$$

where $a_{*S^{2-}}^m$ is the activity of the $^*S^{2-}$ species in the melt; f_i is the fugacity of species i in the coexisting vapour; $\gamma_{*S^{2-}}^m$ is the activity coefficient of species $^*S^{2-}$ in the melt; and $w_{*S^{2-}}^m$ is the concentration (as weight fraction) of the $^*S^{2-}$ species in the melt. The equilibrium constant, $K_{*S^{2-}}$, is a function only of P and T—not melt composition—yet the solubility of the $^*S^{2-}$ species in silicate melts is strongly compositionally dependent [e.g. Fincham and Richardson 1954], reflecting the strong compositional dependence of the activity coefficients in Equation 34.

One option is that the overall effects of melt composition are incorporated into the $\gamma_{*S^{2-}}^m(P,T,X)$ function and thus also into the solubility function:

$$C_{*S^{2-}}(P,T,X) = \frac{K_{*S^{2-}}(P,T)}{\gamma_{*S^{2-}}^m(P,T,X)} = w_{*S^{2-}}^m \left(\frac{f_{O_2}}{f_{S_2}} \right)^{0.5}, \tag{35}$$

where $C_{*S^{2-}}$ is the solubility function for $^*S^{2-}$ and the X refers to melt composition. Alternatively, C_i is treated as a capacity,

as is commonly used for sulfide and sulfate [e.g. Fincham and Richardson 1954; Spera and Bergman 1980; O'Neill 2021]. In other words, a separate equilibrium constant can be written for the reaction between $^{*}S^{2-}$ and each of the oxide components in the melt:

$$0.5S_2(v) + CaO(m) \rightleftharpoons CaS(m) + 0.5O_2(v)$$
$$K^{CaO}_{*S^{2-}}(P,T) = \frac{w^m_{CaS}}{w^m_{CaO}}\left(\frac{f_{O_2}}{f_{S_2}}\right)^{0.5}, \quad (36)$$

$$0.5S_2(v) + FeO(m) \rightleftharpoons FeS(m) + 0.5O_2(v)$$
$$K^{FeO}_{*S^{2-}}(P,T) = \frac{w^m_{FeS}}{w^m_{FeO}}\left(\frac{f_{O_2}}{f_{S_2}}\right)^{0.5}, \quad (37)$$
$$\text{etc.}$$

The capacity is then the concentration-weighted sum of the K_i's for each component [e.g. Fincham and Richardson 1954; Spera and Bergman 1980; O'Neill 2021]:

$$C_{*S^{2-}}(P,T,X) = \sum_{i=1}^{n} w^m_i \cdot K^i_{*S^{2-}}(P,T) = w^m_{CaO} \cdot K^{CaO}_{*S^{2-}}(P,T) + w^m_{FeO} \cdot K^{FeO}_{*S^{2-}}(P,T) + \text{etc.}, \quad (38)$$

where i is a melt component.

The key point about using this approach is that the dependence of volatile solubility on P, T, and melt composition can be parameterised relatively straightforwardly given sufficient experimental data on the solubility of each volatile species as a function of melt composition. However, there is no universal functional form for the solubility functions in `VolFe`. In some cases, they are assumed to be constant (i.e. independent of P, T, and/or melt composition); a linear combination of oxide concentrations; or vary as functions of composition based on thermodynamic constraints or alternative empirical formulation. A variety of parameterisations for the solubility functions in terms of P, T, and X are available in the current version of `VolFe`. These are taken from the literature, which have been benchmarked where possible (worked calculations are available as Jupyter Notebooks on the GitHub repository and ReadTheDocs), and in a few cases we have derived new parameterisations from literature data described in the Supplementary Material (a full list of parameterisations included in `VolFe` is given in Supplementary Material Tables S3–8). Additional parameterisations can be added as new experimental data and parameterisations become available for all species (an example of this is shown in the ReadTheDocs).

Of particular importance for all models of volatile solubility and degassing is the strong dependence of the solubility of CO_2 (i.e. $CO_{2,T}$) on melt composition [e.g. Blank and Brooker 1994; Shishkina et al. 2014; Wieser et al. 2022a]. Parameterisations of $CO_{2,T}$ solubility currently available in `VolFe` from the literature (see full list in Supplementary Material Table S3) are each typically valid over a narrow range of melt composition, with the range of all included parameterisations ranging from MORB through to alkali-rich compositions such as leucitite [Holloway and Blank 1994; Thibault and Holloway 1994; Dixon et al. 1995; Dixon 1997; Lesne et al. 2011a], and for rhyolite [Blank et al. 1993]. To then speciate $CO_{2,T}$ as $CO_{2,mol}$ and CO_3^{2-} in `VolFe`, current options for the equilibrium constant for Equation 20 are for basalt (all CO_3^{2-}), andesite or dacite (both CO_3^{2-} and $CO_{2,mol}$ [Botcharnikov et al. 2006]), and rhyolite (all $CO_{2,mol}$) (Supplementary Material Table S4). Note that currently, the effect of H_2O on CO_2 solubility is not included [e.g. King and Holloway 2002; Papale et al. 2006; Iacono-Marziano et al. 2012].

The solubility function for H_2O_T is far less dependent on melt composition than $CO_{2,T}$ over the compositional range of abundant natural magmas [e.g. Moore et al. 1998; Lesne et al. 2011b; Iacono-Marziano et al. 2012; Allison et al. 2022]. Currently in `VolFe`, there are representative values for the solubility functions of basalt (Hughes et al. [2024], using data from the compilation of Allison et al. [2022]) and rhyolite (derived in Supplementary Material Section S1.1 and Figure S1 using data from Kadik et al. [1972], Silver et al. [1990], and Blank et al. [1993]) (Supplementary Material Table S5).

There is limited experimental data for the solubility of CO, CH_4, and H_2 in natural silicate melt compositions. Parameterisations currently available in `VolFe` are for H_2 in basalt and andesite (Hughes et al. [2024], using data from Hirschmann et al. [2012]); CO in basalt (Hughes et al. [2024], using data from Wetzel et al. [2013], Stanley et al. [2014], and Armstrong et al. [2015]), and CH_4 in basalt [Ardia et al. 2013] (Supplementary Material Table S8).

There is a wealth of experimental data that have been used to parameterise the solubility functions (often called capacities) for $^{*}S^{2-}$ [O'Neill 2021; Boulliung and Wood 2023b] and SO_4^{2-} [Boulliung and Wood 2022; O'Neill and Mavrogenes 2022; Boulliung and Wood 2023a; b], which have been included in `VolFe` (Supplementary Material Table S6–7). These cover a wide range of melt compositions (basalts through rhyolite) and T, but not P (although some parameterisations include a P dependence). For the H_2S solubility function in `VolFe`, parameterisations are given in Hughes et al. [2024] for basalt and basaltic andesite based on data from Lesne et al. [2015] and Moune et al. [2009] (Supplementary Material Table S8).

Parameterisations for the solubility functions for inert atomic species are included in `VolFe` for Ar and Ne in basalt or rhyolite using data from Iacono-Marziano et al. [2010] (Supplementary Material Section S1.1, Figure S2, and Table S8). The user can also just type a numerical value to use as the solubility function (i.e. a constant) within the `VolFe` framework.

3.5 Treatment of fO_2, Fe^{3+}/Fe_T, and total oxygen content

The final linearly independent equilibrium is one that describes equilibrium between FeO and $FeO_{1.5}$. We have chosen the widely utilised, heterogeneous melt-vapour equilibrium for this purpose [e.g. Sack et al. 1981] given as Equation 21 in Table 3.

Several parameterisations for the relationship between fO_2 and Fe^{3+}/Fe^{2+} in the melt covering a wide range of P, T, and

melt composition are available in VolFe [Kress and Carmichael 1991; Borisov et al. 2018; O'Neill et al. 2018, Supplementary Material Table S9], which have been benchmarked where possible (worked calculations are available as Jupyter Notebooks on the GitHub repository and ReadTheDocs).

By including Equation 21, VolFe returns the values of fO_2 and Fe^{3+}/Fe^{2+} of the equilibrium state of the system. For some calculations using VolFe, fO_2 or Fe^{3+}/Fe^{2+} are taken as independent variables (e.g. determination of P^v_{sat} described in Section 4.1). In such cases, the bulk oxygen content of the system varies depending on the values of the independent variables. For other calculations (e.g. closed-system degassing described in Section 4.3), fO_2 or Fe^{3+}/Fe^{2+} are dependent variables that vary with the path of the independent variables because the bulk O content of the system is conserved. Currently, VolFe does not include the option to externally buffer the fO_2 (e.g. maintain the system at a given ΔFMQ during degassing) where the system is open to oxygen [e.g. CHOSETTO; Moretti and Ottonello 2003; Moretti and Papale 2004].

Only one fO_2-dependent variable (fO_2, Fe^{3+}/Fe_T, or S^{6+}/S_T) can be chosen as an independent variable in calculations currently implemented in VolFe. If the user specifies more than one such fO_2-dependent variable as independent, a warning will be raised and VolFe will alert the user to its choice of a single independent fO_2-dependent variable.

3.6 Sulfide, anhydrite, and graphite

Given the conditions (P, T, fO_2) and compositions of the melt ± vapour, VolFe can determine whether the system is supersaturated with respect to sulfide, anhydrite, and/or graphite. This is done by comparing the $^*S^{2-}$ content of the melt to the sulfide content at sulfide saturation (S^{2-}CSS, Equation 39); the S^{6+} content of the melt to the sulfate content at anhydrite saturation (S^{6+}CAS, Equation 40); and the (fCO_2/fO_2) ratio of the vapour to the equilibrium constant for graphite formation (Equation 41) (Table 4). If the silicate melt is supersaturated with respect to any of these phases (i.e. Equation 39, 40, or 41 are satisfied), the calculated coexisting silicate melt and vapour compositions are metastable relative to an assemblage containing one or more of these phases. In this case, as in Hughes et al. [2023b], VolFe can limit the sulfur or carbon content of the silicate melt to that at the saturation condition (i.e. satisfy the equations in Table 4). For graphite, this is equivalent to graphite precipitation, although the amount of graphite that forms is not calculated. For sulfide liquid and anhydrite, this would only approximate their precipitation because the non-volatile melt composition does not change in the VolFe calculation even though in reality it would (i.e. the FeO and CaO of the silicate melt should change) and the amount of the sulfide liquid and anhydrite phases are not calculated.

For graphite, the parameterisation of the equilibrium constant from Holloway et al. [1992] is available in VolFe (Supplementary Material Table S10). For the S^{2-}CSS, VolFe assumes the sulfide liquid phase is pure FeS unless concentrations of Fe, Cu, and/or Ni in the sulfide are specified by the user (note that not all parameterisations account for the presence of Cu or Ni). There are several different parameterisations from the literature for S^{2-}CSS and S^{6+}CAS available in the current version of VolFe (some of which have been benchmarked: worked calculations are available as Jupyter Notebooks on the GitHub repository and ReadTheDocs); these cover a wide range of P, T, and melt compositions for the S^{2-}CSS [Liu et al. 2007; Fortin et al. 2015; Smythe et al. 2017; Liu et al. 2021; O'Neill 2021; O'Neill and Mavrogenes 2022] and S^{6+}CAS [Chowdhury and Dasgupta 2019; Zajacz and Tsay 2019], mostly implemented using the PySulfSat Python package [Wieser and Gleeson 2023] for their calculation (Supplementary Material Table S10).

Table 4: Saturation conditions for sulfide, anhydrite, and graphite.

Phase	Saturation condition	
Sulfide	$S^{2-}\text{CSS} = w^m_{*S^{2-}}$	(39)
Anhydrite	$S^{6+}\text{CAS} = w^m_{S^{6+}}$	(40)
Graphite	$K_G = \frac{f_{CO_2}}{f_{O_2}}$	(41)

S^{2-}CSS = sulfide content at sulfide saturation;
S^{6+}CAS = sulfate content at anhydrite saturation;
w^m_i = weight fraction in the melt of species i;
f_i = fugacity of species i;
K_G = equilibrium constant for $C_G(s) + O_2(v) = CO_2(v)$.

4 Calculation types in VolFe

Given the thermodynamic framework and model-dependent variables (Section 3), VolFe calculates the equilibrium state of the system given the choice of independent variables. As emphasised throughout, different calculation types are possible by choosing different independent variables. In the current implementation of VolFe, T is always one of the independent variables and is set by the user. Here we outline the three main types of calculations [e.g. Hughes et al. 2023b; 2024], as well as some additional potentially interesting calculations, currently addressable using functions built into VolFe as illustrated in Figure 2. Details of exactly how to implement the calculations and worked examples are given in the ReadTheDocs as Jupyter Notebooks, which are also available on the GitHub repository (a brief overview of what is currently available is given in Supplementary Material Section S4).

The required inputs for each calculation are detailed in the following subsections. Volatile concentrations are specified as the equivalent amounts of total hydrogen as H_2O (termed H_2O-eq, wt.%), total carbon as CO_2 (CO_2-eq, ppmw), and total sulfur (S_T, ppmw). The total amount of the "X" component is simply referred to as "X" (ppmw) since there is only a single melt and vapour "X"-bearing species. For the calculations, the volatile contents (i.e. the absolute values of H_2O-eq, CO_2-eq, S_T, and "X") are used directly as inputted, whilst the volatile-free melt composition (SiO_2, TiO_2, etc.) is recalculated such that is sums to 100 wt.% minus the sum of the total volatiles (example in Supplementary Material Table S12).

We illustrate the use of VolFe in understanding natural systems by applying the calculations described in this section to data from the Marianas arc [Kelley and Cottrell 2012;

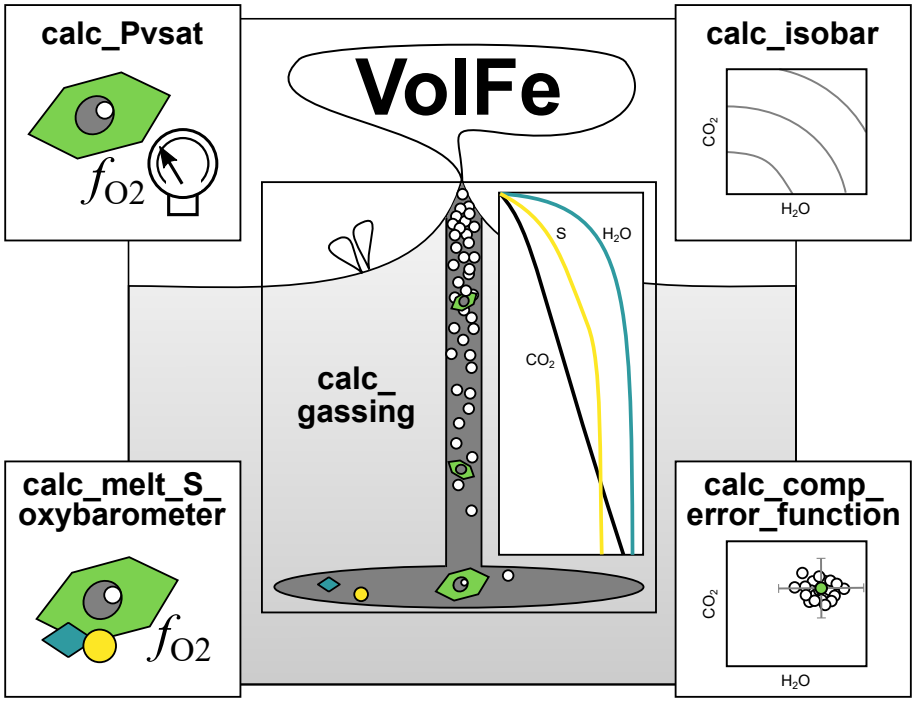

Figure 2: Schematic figure showing the key functions in `VolFe`: `calc_Pvsat` = calculate the pressure of vapour-saturation for a given melt composition and T (Section 4.1); `calc_isobar` = calculate varying H_2O-CO_2 concentrations at a given P and T (Section 4.2); `calc_gassing` = calculate isothermal open- and closed-system degassing and regassing paths (Section 4.3); `calc_melt_S_oxybarometer` = calculate the fO_2 range for a given melt composition based on the sulfur content assuming sulfide- and anhydrite-saturation (Section 4.4); and `calc_comp_error_function` = Monte Carlo approach to generate melt compositions within analytical error and run them through `calc_Pvsat` or `calc_melt_S_oxybarometer` (Section 4.5).

Brounce et al. 2014], using the Fe^{3+}/Fe_T values from Cottrell et al. [2021] where available that have been recalculated using the updated Mössbauer-XANES calibration of Zhang et al. [2018]. These data were chosen because they have CO_2-eq, H_2O-eq, S, Fe^{3+}/Fe_T, and major element composition measured for each olivine-hosted basaltic melt inclusion glass (MI, n = 49; Arigan = circle, Sarigan = triangle, and Alamagan = square) and basaltic-andesite submarine pillow glass (SPG, n = 2; Southern Mariana Trough = diamond), which are required inputs for most `VolFe` calculations (e.g. measured composition in Figure 3). See Supplementary Material Table S13 for species and model dependent variables used in the calculations. We recommend that the original reference for the specific parameterisations of the model-dependent variables used within the `VolFe` calculations be clearly cited. Additionally, if the parameterisation is implemented in `VolFe` using an external `Python` package this should also be cited (e.g. S^{2-}CSS using `PySulfSat` by Wieser and Gleeson [2023]; melt density using `DensityX` by Iacovino and Till [2019]). The T chosen for each glass composition was calculated based on the measured volatile-free melt composition and H_2O-eq using Equation 14 from Putirka [2008] as implemented in `Thermobar` [v1.0.41; Wieser et al. 2022b] (Figure 4A). These calculated T (Figure 4A) were then used in the `VolFe` calculations presented here, all of which used `VolFe` v1.0.0. A Jupyter notebook for this full workflow is in the GitHub repository and ReadTheDocs and can be used as a template for data processing.

4.1 The pressure of vapor-saturation of a magma and its use as a geobarometer

The dissolved volatile contents of a melt in equilibrium with a vapour can be used as a barometer because the sum of the partial pressures of all the vapour species (P^v_{sat}) must equal the total pressure (Equation 10) [e.g. Anderson Jr et al. 1989; Blundy and Cashman 2008; Hughes et al. 2024]. Calculations of P^v_{sat} have been widely applied to melt inclusions to calculate magma storage depths [e.g. Colman et al. 2015; Wanless et al. 2015; Camejo-Harry et al. 2018; 2019; Black and Andrews 2020; Wieser et al. 2021] and to sub-aqueous matrix glasses to calculate eruption depths [e.g. Seaman et al. 2004; Coombs et al. 2006; Lund et al. 2018; Belgrano et al. 2021]. As the phase proportions are not required, the phase rule defines the number of independent variables required (Equation 2: F = 2–5 depending on the number of volatile species in the system). The independent variables used in `VolFe` for this calculation are T; the total concentrations of C, H, S, and/or "X" in the melt (depending on which volatiles are present in the system); and an fO_2-dependent variable (e.g. fO_2, Fe^{3+}/Fe_T, or S^{6+}/S_T). From this, P^v_{sat}, the melt speciation (i.e. concentrations of the various dissolved melt species), and the vapour composition and speciation are calculated. This calculation is outlined in detail in Hughes et al. [2024] (Figure 5). In brief, the pressure and melt speciation are iteratively calculated until the sum of the partial pressures of all the vapour species equals the total pressure (i.e. Equation 10 is satisfied).

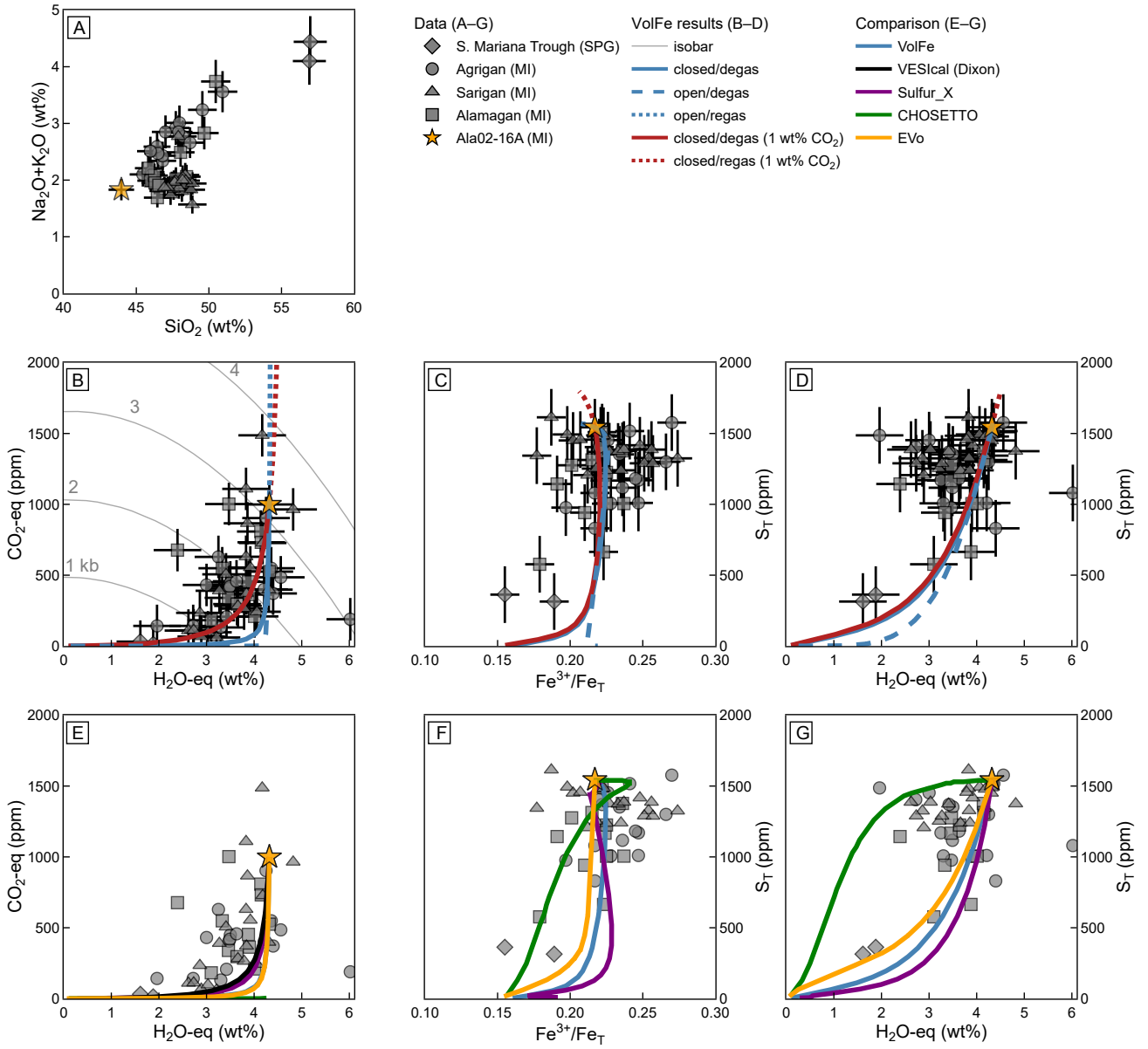

Figure 3: Measured melt inclusion (MI) and submarine pillow glass (SPG) data from the Marianas arc [Kelley and Cottrell 2012; Brounce et al. 2014; Cottrell et al. 2021] and modelling results using VolFe and some other available tools: [A] normalised SiO_2 vs. normalised total alkalis (Na_2O+K_2O); [B], [E] CO_2-eq vs. H_2O-eq; [C], [F] S_T vs. Fe^{3+}/Fe_T; and [D], [G] S_T vs. H_2O-eq. Symbols are measured data (grey), where the shape indicates MI or SPG and volcano with 2 sigma errors bars (diamond = Southern Mariana Trough SPG, circle = Agrigan MI, square = Sarigan MI, triangle = Alamagan MI, and yellow star = Ala02-16A MI). Isobars (grey curves) are shown in [B] for Ala02-16A. Re- and degassing paths are shown in [B]–[D] starting from the composition of Ala02-16A assuming: closed-system degassing (blue solid); closed-system degassing (red solid) and regassing (red dot) with 1 wt.% initial CO_2; and open-system degassing (blue dash) and regassing (blue dot). The closed-system degassing calculation where the MI Ala02-16A represents the bulk composition (i.e. the solid blue curve in [B]–[D]) for VolFe (blue: under the orange-Evo curve in [E]), VESIcal (Dixon, black—[E] only), Sulfur_X (purple), CHOSETTO (green: essentially along the x-axis in [E]), and EVo (orange) are shown in [E]–[G] (error bars are omitted in these panels for clarity).

As an example, P^v_{sat} and fO_2 were calculated for each glass composition from the Marianas dataset (Figure 4A–4B). Note that these studies only measured the CO_2 content of the glass within the melt inclusion and did not measure the CO_2 content of any coexisting vapour bubbles [Kelley and Cottrell 2012; Brounce et al. 2014]. This means the total CO_2 content of the melt inclusions is likely underestimated, which means entrapment pressures of the melt inclusions will be underestimated if assumed to equal P^v_{sat} [Hartley et al. 2014; Moore et al. 2015; Wallace et al. 2015; Wieser et al. 2021]. Hence, more accurate entrapment pressures using P^v_{sat} will be calculated from melt inclusion data where CO_2 in both the glass

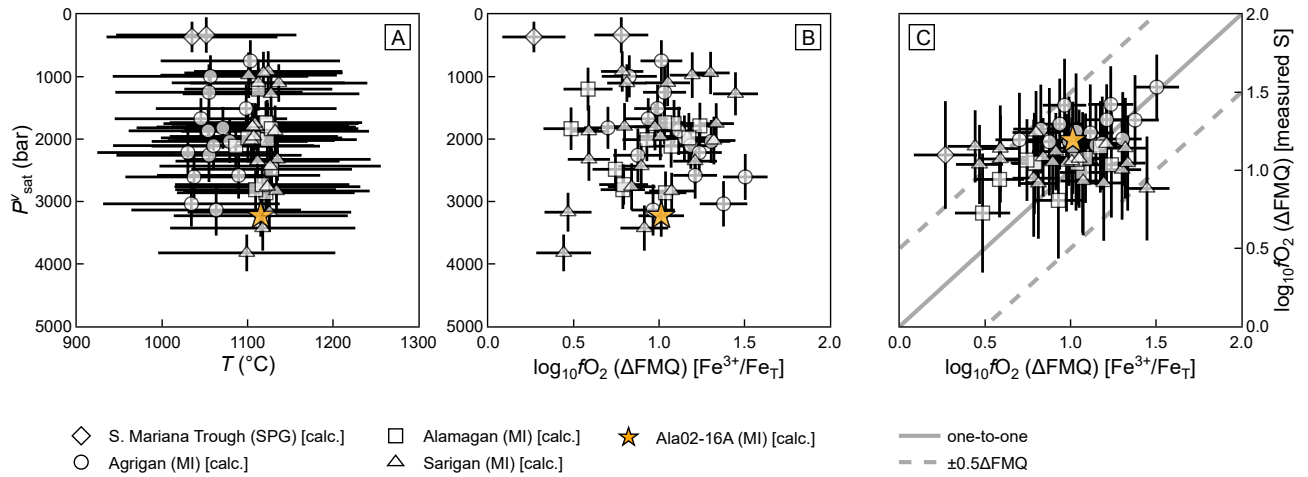

Figure 4: Results for the pressure of vapour-saturation barometer calculations using measured Fe^{3+}/Fe_T (Section 4.1) for the Marianas dataset showing calculated P^v_{sat} vs. [A] calculate T using Equation 14 from Putirka [2008] implemented in `Thermobar` [Wieser et al. 2022b]; and [B] calculated ΔFMQ from Fe^{3+}/Fe_T. [C] Calculated ΔFMQ using measured sulfur concentration vs. calculated ΔFMQ using measured Fe^{3+}/Fe_T, where the solid line is the one-to-one relationship and dotted lines are ±0.5ΔFMQ. Symbol shape indicates MI or SPG and volcano (diamond = Southern Mariana Trough SPG, circle = Agrigan MI, square = Sarigan MI, triangle = Alamagan MI, and yellow star = Ala02-16A MI), which are white as all values are calculated rather than measured. Associated error bars are 2 sigma values based on calculations using 100 compositions generated from a Monte Carlo approach (see text for details).

and bubble is measured and combined to calculate the melt content at entrapment.

4.2 Isobars

Vapour-saturated isobars are curves or surfaces of vapour-saturated melt compositions for a fixed volatile-free base melt composition at a given P^v_{sat}. Typically, they are shown as the loci of pairs of experimentally-determined or model-calculated concentrations of H_2O_T and $CO_{2,T}$ in vapour-saturated melt at a single P (and T) but spanning $H_2O/(H_2O + CO_2)$ from 0 to 1 in the vapour. Such diagrams have been widely used to compare the H_2O_T and $CO_{2,T}$ concentrations on these isobars to measured values in melt inclusions and matrix glasses to estimate P^v_{sat} at entrapment for melt inclusions and eruption for the matrix glasses [e.g. Dixon and Stolper 1995]. Such determinations are subject to a variety of caveats [e.g. Wieser et al. 2022a].

`VolFe` can be used to calculate such isobars at a given T and volatile-free melt composition assuming the melt only contains H_2O_T and $CO_{2,T}$ and the vapour only contains H_2O and CO_2. For each P, first `VolFe` calculates the $CO_{2,T}$ content of the melt with no H_2O_T present and the concentration of H_2O_T in the melt with no $CO_{2,T}$ present. Next, at 20 equal intervals of H_2O_T concentration in the melt between 0 and the maximum H_2O_T, `VolFe` calculates the associated p_{H2O}. Then, p_{CO2} is calculated from $(P - p_{H2O})$, and finally the $CO_{2,T}$ concentration in the melt is calculated. As an example, we used the composition of Ala02-16A (i.e. measured volatile-free melt composition and calculated T; Fe^{3+}/Fe_T and S are not included in this calculation) to calculate isobars for varying H_2O_T and $CO_{2,T}$ at 1000–4000 bar in 1000 bar increments (Figure 3B). Additionally, a comparison to isobars calculated using the Dixon [1997] model in `VESIcal` [Iacovino et al. 2021] are shown in Supplementary Material Figure S4, with a Jupyter Notebook for the calculation available on the GitHub repository and ReadTheDocs.

4.3 Degassing and regassing paths

The main application we envision for `VolFe` is calculation of the compositions (including Fe^{3+}/Fe_T and therefore fO_2) and mass fractions of coexisting melt and vapour during magma degassing. For these calculations, the bulk composition of the system is specified, and P and T are the independent variables. Currently, `VolFe` only considers isothermal paths of vapour-saturated melt (i.e. varying P at constant T), which could be adapted in the future. We refer to paths of decreasing P where vapour-saturated melt ascends as "degassing", resulting in progressive exsolution of volatiles from melt into vapour. The reverse occurs (i.e. progressive dissolution into the melt of volatiles in the vapour) with increasing P; we refer to this as "regassing". Regassing can happen in nature when subaerial, vesicular lava flows enter the ocean causing bubble resorption [e.g. Moore et al. 1985] or in downward limbs of a convecting bubbly magma chambers and conduits [e.g. Carey et al. 2013]. The concept of regassing can also be used to reconstruct the undegassed (or less degassed) volatile contents of parental magmas. `VolFe` also allows the bulk composition of the system to be varied in successive steps (e.g. by removal or by addition of the vapour in equilibrium with melt at each step) to simulate open-system behaviour. Melt density is calculated using `DensityX` [Iacovino and Till 2019] in `VolFe` along these P-T paths.

The exact way in which the equations are solved for these processes by `VolFe` depends on the number of vapour species

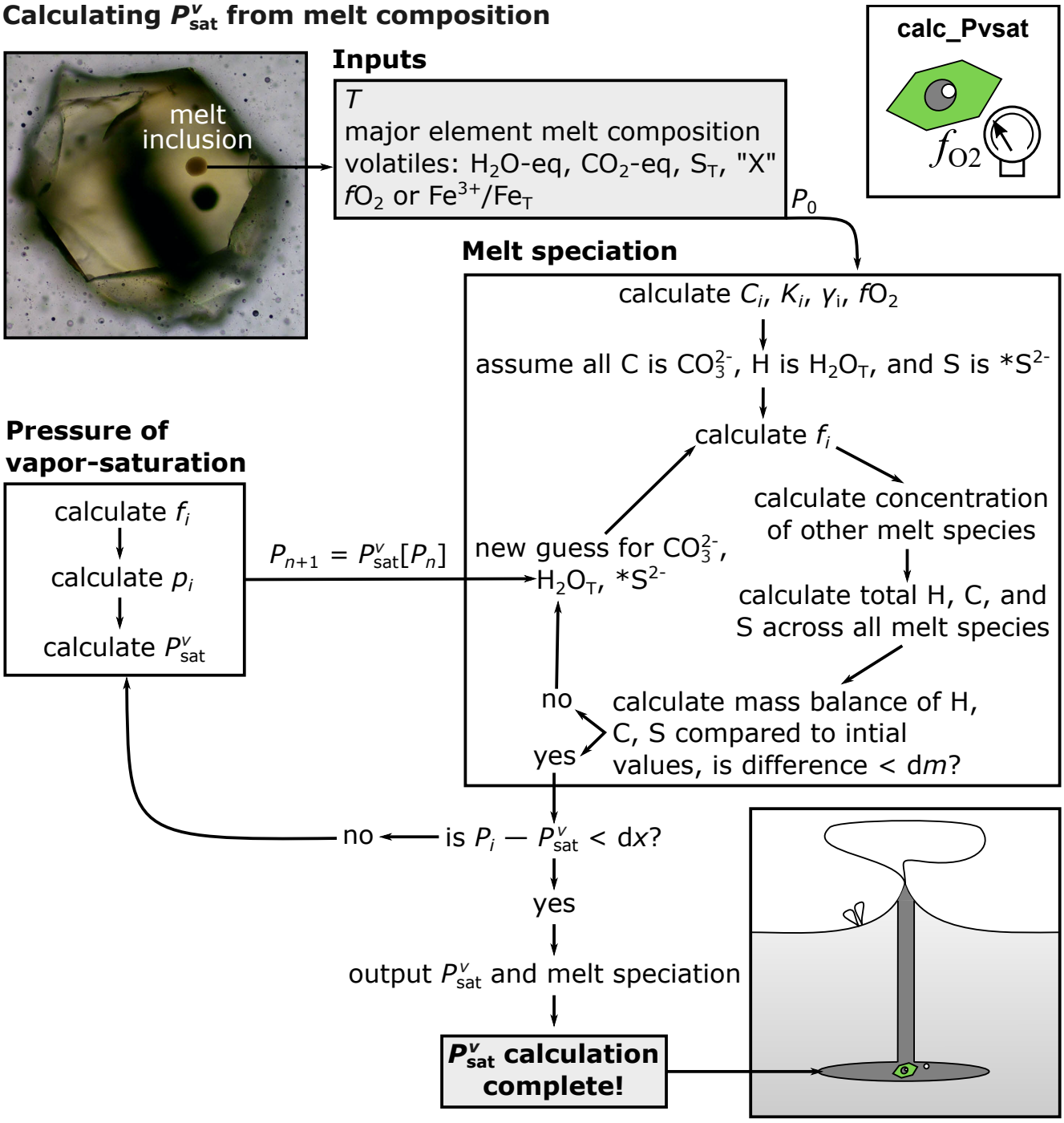

Figure 5: Flow chart describing the calculation of the pressure of vapour-saturation. Adapted from the Supplementary Material of Hughes et al. [2024]. *Abbreviations:* P^v_{sat} = pressure of vapour saturation; T = temperature; H_2O-eq = equivalent amount of H as H_2O; CO_2-eq = equivalent amount of C as CO_2; S_T = total sulfur; P_0 = initial P guess; P_n = P at iteration n; C = solubility function; K = equilibrium constant; γ = fugacity coefficient; f = fugacity; p = partial pressure; dm = mass balance tolerance; and dx = P tolerance.

assumed to be present but is the same for closed- and open-system regassing and degassing calculations. Here, we describe briefly the calculations for a magma containing COHS-bearing volatile species (i.e. all ten vapour species, except "X"; Figure 6). Each step is solved for a given bulk composition of the system at fixed values of P and T. Given reasonable starting guesses for the mole fractions of three independent vapour species (e.g. O_2, CO, and S_2), the concentrations of all other melt and vapour species can be calculated iteratively from the homogeneous vapour and heterogeneous melt-vapour equilibria in Equation 3–8 and Equation 11–19. Using these calculated vapour concentrations and the mass balances for C, H, O, and S across melt and vapour, we calculate the weight fraction of vapour based on each volatile element (Equation 22–

33). The "solver" currently uses the Jacobian matrix/Newton-Raphson approach and the differential equations were generated using `SymPy` [Meurer et al. 2017] from the equations in Section 3.3 (a Jupyter Notebook for generating the differential equations is available in the GitHub repository). The values for the mole fractions of the "guessed" vapour species are then updated in successive iterations until the difference in estimates of vapour weight fraction from each volatile element are within a specified tolerance (typically 10^{-9} weight fraction). The mole fraction of O_2 is always one of the "guessed" species to ensure numerical convergence as it has a small absolute value and would be difficult to calculate subsequently via mass balance (further discussion in Supplementary Material Section S3). Crucial to this approach is good initial guesses of the three vapour mole fractions at each P-step. We use values from the previous calculation step as initial guesses, which is particularly useful at the start of the degassing calculation as we can use the values at P^v_{sat} as starting guesses for the first P-step. Currently, the initial P that `VolFe` starts re- and degassing calculations is always the P^v_{sat} of the given melt composition (i.e. the user cannot specify the initial P). Further details of our approach are provided in Supplementary Material Section S3.

Note that this specific calculation in `VolFe` requires using the relationship between fO_2 and Fe^{3+}/Fe^{2+} from equations A-5, 6 in Kress and Carmichael [1991] (i.e. the other parameterisations in Supplementary Material Table S9 cannot be used currently). Equations A-5, 6 were chosen due to their thermodynamic formulation rather than the empirical form of the more widely used Equation 7 from Kress and Carmichael [1991]. Results using equations A-5, 6 are expected to be similar to those using Equation 7 because Kress and Carmichael [1991] report that both reproduce the input experimental data equally well (standard errors of 0.33 and 0.37 wt.% for FeO and Fe_2O_3, respectively, for equations A-5, 6 compared to 0.21 and 0.42 wt.% for Equation 7) and results using both equations are essentially indistinguishable in Figure 3 of Kress and Carmichael [1991].

For closed-system calculations, the bulk composition of the system remains constant (i.e. the bulk concentrations of C, O, S, H, "X", and silicate component); the evolving melt and vapour remain in chemical equilibrium throughout; and regassing is simply the reverse of degassing. For open-system degassing, the vapour is removed at each P-step and the melt composition becomes the bulk composition of the system for the next step. For open-system regassing, a small increment of vapour that is in equilibrium with the melt is added to the system defining a new bulk composition (the amount of vapour can be user-defined). This procedure can be calculated *ad infinitum*, but in practice it would be stopped at some point defined by constraints external to the `VolFe` calculations (e.g. at a particular P, CO_2, H_2O, etc. content believed reasonable based on other petrological arguments: currently it stops at a user-defined P). This open-system regassing calculation is precisely analogous to correcting for fractional crystallisation of olivine from a parental melt for an evolved basalt that only has olivine on its low-P liquidus. Hence, open-system regassing can be used to reconstruct the initial composition of a parental or even primary melt.

Both open- and closed-system regassing and degassing calculations in `VolFe` require a T and an initial melt composition (i.e. the volatile-free melt composition, CO_2-eq, H_2O-eq, S_T and/or "X", and fO_2 value or measured Fe^{3+}/Fe_T or S^{6+}/S_T) from which to start the calculation. For a glassy pillow rim from the sea floor, the required melt composition could simply be taken as the measured glass composition. For a melt inclusion, the required melt composition could be the bulk composition of the melt inclusion at the time of entrapment (i.e. correcting for vapour bubble formation, post-entrapment crystallisation, etc.; e.g. Rose-Koga et al. [2021]). Regardless of how it is obtained, this melt composition fixes the bulk composition of the system if there is no vapour present. This is always the starting condition for open-system regassing and degassing calculations and can be the starting condition for closed-system degassing calculations.

Alternatively, the melt composition at the start of the calculation might coexist with a vapour (e.g. in an ascending magma in which degassing had already begun). Coexisting melt and vapour must be the starting condition for closed-system regassing and could be the starting condition for closed-system degassing. If the amount of coexisting vapour prior to increasing or decreasing P is known or estimated, this can be specified as an input in `VolFe`: `VolFe` then calculates the composition of this equilibrium vapour at P^v_{sat} given the specified melt composition (e.g. Section 4.1). The bulk composition of the system is then calculated as the weighted combination of the compositions of coexisting melt and vapour and the starting point for the calculation is a melt+vapour assemblage. However, the amount of vapour is often unknown. In such cases, it might be possible to estimate the bulk CO_2 content of the undegassed magma [e.g. Macpherson and Mattey 1994; Moore and Bodnar 2019]. The amount of vapour present can then be calculated given mass balance between the carbon in the melt and vapour at P^v_{sat} (the composition of the melt is known and the composition of the vapour is calculated as in Section 4.1 and the initial carbon (Equation 22–25). From this, the initial composition of all volatiles can be calculated and therefore the bulk composition of the system specified.

For closed-system calculations, the bulk composition of the system (including O) is fixed. The constancy of total O results in systematic variations in all dependent variables with progressive re- and degassing, because fO_2, Fe^{3+}/Fe_T and S^{6+}/S_T are all dependent variables. For `VolFe`, open-system does not mean the system is open only to O, as would be the case if fO_2 were fixed (e.g. buffered) externally. As with closed-system calculations, the changing composition of the system at each step during open-system calculations results in continuous variations in fO_2 and Fe^{3+}/Fe_T and S^{6+}/S_T because these are dependent variables.

At each P-step for open- or closed-system regassing or degassing, the calculated equilibrium melt composition is checked for saturation with respect to graphite, liquid sulfide, and/or anhydrite (see Section 3.5). If the melt composition is supersaturated with respect to one or more of these phases, the

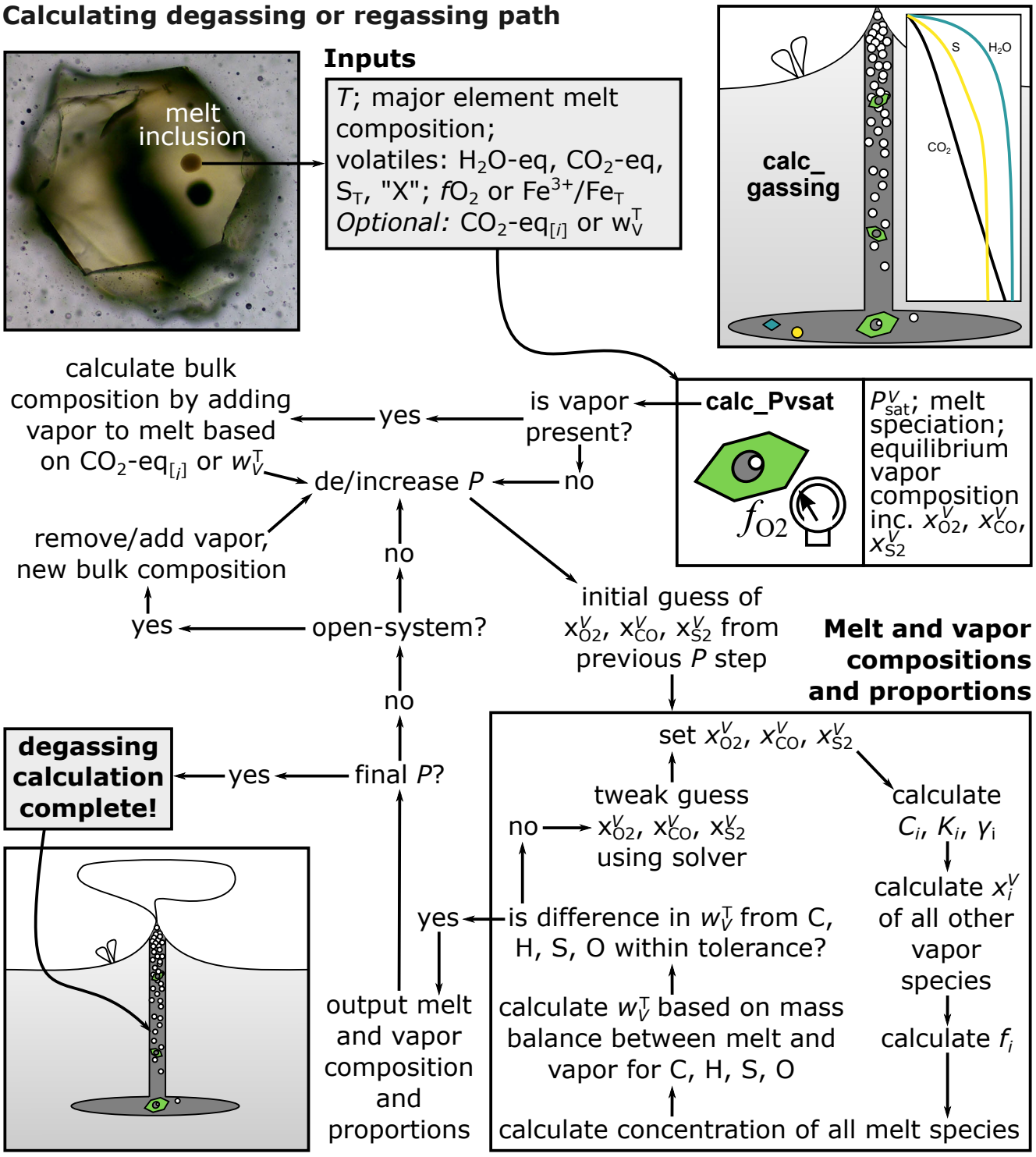

Figure 6: Flow chart describing the re/degassing calculation. Abbreviations: P^v_{sat} = pressure of vapour-saturation; P = pressure; T = temperature; H_2O-eq = equivalent amount of H as H_2O; CO_2-eq = equivalent amount of C as CO_2; S_T = total sulfur; CO_2-eq$_{[i]}$ = bulk CO_2-eq concentration of the system if different to CO_2-eq; w^T_v = weight fraction of the vapour; x^v_i = mole fraction in the vapour; C = solubility function; K = equilibrium constant; γ = fugacity coefficient; and f = fugacity.

user can specify that the carbon and/or sulfur content of the melt is capped at the value of saturation (e.g. the $^*S^{2-}$ content of the melt is equal to S^{2-}CSS; Section 3.4) and the equilibrium state of the system is found at this capped sulfur and/or carbon content. However, the major element composition of the melt does not change to account for sulfide and/or anhdyrite formation (i.e. Fe and Ca do not change). In this case, the "excess" S and/or C from the previous step (e.g. for sulfide supersaturation, this is the difference in $^*S^{2-}$ between the metastable supersaturated melt $^*S^{2-}$ content and that of sulfide-saturated

melt for the same base melt composition) is sequestered for consideration in the next *P*-step. For open-system calculations, the additional C and/or S are then removed from the system for the next *P*-step. For closed-system calculations, if the S and/or C content of the melt drops below graphite, liquid sulfide, and/or anhydrite saturation at a subsequent *P*, the sequestered C and/or S are added back to the system. This treatment of supersaturation is crude and involves a variety of approximations. However, given the small amounts of sulfide and/or anhydrite that are likely to precipitate for natural systems, and therefore the small change in major element melt composition, we feel this simplified treatment is likely to give reasonable results.

As an example, we calculated various closed- and open-system regassing and degassing paths with Ala02-16A as the starting melt composition (i.e. measured glass composition has 999 ppm CO_2-eq, 4.52 wt.% H_2O-eq, 1544 ppm S_T, and 0.238 Fe^{3+}/Fe_T, volatile-free melt composition, and the calculated T is 1111 °C): (1) isothermal closed-system degassing with no vapour present at the start of degassing; (2) isothermal open-system degassing; (3) isothermal open-system regassing; and isothermal closed-system (4) degassing and (5) regassing where the bulk system contains 1 wt.% CO_2 (i.e. vapour is present at the yellow star) (Figure 3B–3D). Regassing calculations went up to 5000 bar and could be used to estimate the composition and P^v_{sat} of permissible parental liquids from which the entrapped melt inclusion glasses formed by degassing. For comparison to the degassing paths, we plot the measured (grey symbols: CO_2-eq, H_2O-eq, S_T, and Fe^{3+}/Fe_T) or calculated at P^v_{sat} (white symbols: S^{6+}/S_T, ΔFMQ, and vapour composition) values for the individual melt inclusion and submarine pillow glass analyses (Figure 3, Figure 7, and Figure 8). However, the glasses come from different volcanoes and are therefore not related by simple re- and degassing processes [Kelley and Cottrell 2012; Brounce et al. 2014] and melt composition and T are not constant for the melt inclusion and submarine pillow glass data but are for the calculated re- and degassing paths.

4.4 The "total melt sulfur oxybarometer" based on the sulfur contents of melts and glasses

Oxygen fugacity is a key thermodynamic parameter in magmatic systems because of its effects on the chemical and physical properties of the melt, the crystallisation sequence and liquid line of descent, the speciation of magmatic gases, etc. [e.g. Carmichael and Ghiorso 1990; Kolzenburg et al. 2018; Hughes et al. 2024]. There are many different oxybarometers available and, in certain circumstances, the sulfur content of the melt can be used to place bounds on the fO_2 based on sulfide liquid or anhydrite saturation [e.g. Beermann et al. 2011; Muth and Wallace 2022; Hughes et al. 2023b], using an approach that we term the "total melt sulfur oxybarometer". A short description of its implementation is given here (Figure 9); see Section "Using w^m_{ST} as an oxybarometer" in Hughes et al. [2023b] for a more detailed description.

In `VolFe`, this constraint on fO_2 is implemented by calculating the S^{2-}CSS and S^{6+}CAS for the given conditions (T, P, and melt composition including volatiles). `VolFe` then compares the calculated S^{2-}CSS to the measured sulfur content (S_T). If $S_T > S^{2-}$CSS, it calculates $S^{6+}/S_T = (S_T - S^{2-}CSS)/S_T$ and then converts it to fO_2. If $S_T < S^{2-}$CSS, it cannot calculate a minimum fO_2. A similar comparison is then done for the S^{6+}CAS: if $S^{6+}CAS > S_T$, a maximum fO_2 can be calculated from $S^{6+}/S_T = S^{6+}CAS/S_T$ (no maximum fO_2 can be calculated if $S^{6+}CAS < S_T$). If the calculation is at P^v_{sat} (rather than a specified P), `VolFe` iteratively calculates P and fO_2 until convergence (note that if the specified P is too low for the given volatile content, the melt will be vapour-supersaturated and hence metastable). Hence, if the sulfur content is high enough, for a given T, volatile-free melt composition, and volatile content, a range of allowable fO_2 values can be calculated using `VolFe` (Figure 9).

As an example, the measured S_T content was also used to calculate fO_2 based on the total-melt-sulfur-oxybarometer assuming vapour-saturation for the Marianas dataset (Figure 4C). Only minimum estimates of fO_2 were possible using the measured sulfur content because the sulfur contents were not high enough to be potentially saturated with anhydrite. A few glasses did not have sufficient sulfur for a minimum fO_2 estimate because their sulfur contents are less than S^{2-}CSS (e.g. the two submarine pillow glasses—diamonds—are not shown in Figure 4C).

4.5 Monte Carlo errors for melt composition

Inputs to all these calculations (e.g. oxide concentration, volatile contents, Fe^{3+}/Fe_T, etc.) will have uncertainties associated with them and it can be useful to see how these errors influence the results. A Monte Carlo approach can be applied in `VolFe` to the measured melt composition (and T) assuming absolute or relative errors are independent from each other and normally distributed about a specified mean and standard deviation. These compositions can then be used as starting conditions for the pressure of vapour-saturation and fO_2 from S calculations. While allowing propagation of uncertainty based on user inputs, this approach does not constrain uncertainties introduced by model-dependent variables in `VolFe` (e.g. solubility functions, fugacity coefficients, etc.).

To evaluate the influence of errors associated with measurements of the melt composition on calculated T, P^v_{sat}, and fO_2, we randomly generated 100 different compositions using this Monte Carlo approach for each melt inclusion and submarine pillow glass (Figure 3A–3D). Errors were assumed to be independent and normally distributed with the following one sigma values typical for these types of analyses: ±0.25 wt.% H_2O; ±75 ppm CO_2; ±100 ppm S; ±0.005 Fe^{3+}/Fe_T; ±1% relative for major oxides; ±5% relative for minor oxides, ±51 °C (standard estimate of error of this thermometer: Putirka [2008]) (note that ±2 sigma errors are shown on Figure 3a–d for all species). Each of these 100 compositions was then used to calculate P^v_{sat} and fO_2 (but not degassing paths) as described in sections 4.1 and 4.4 (Figure 4). Including analytical uncertainties from melt composition represents *minimum* uncertainties and does not include model error.

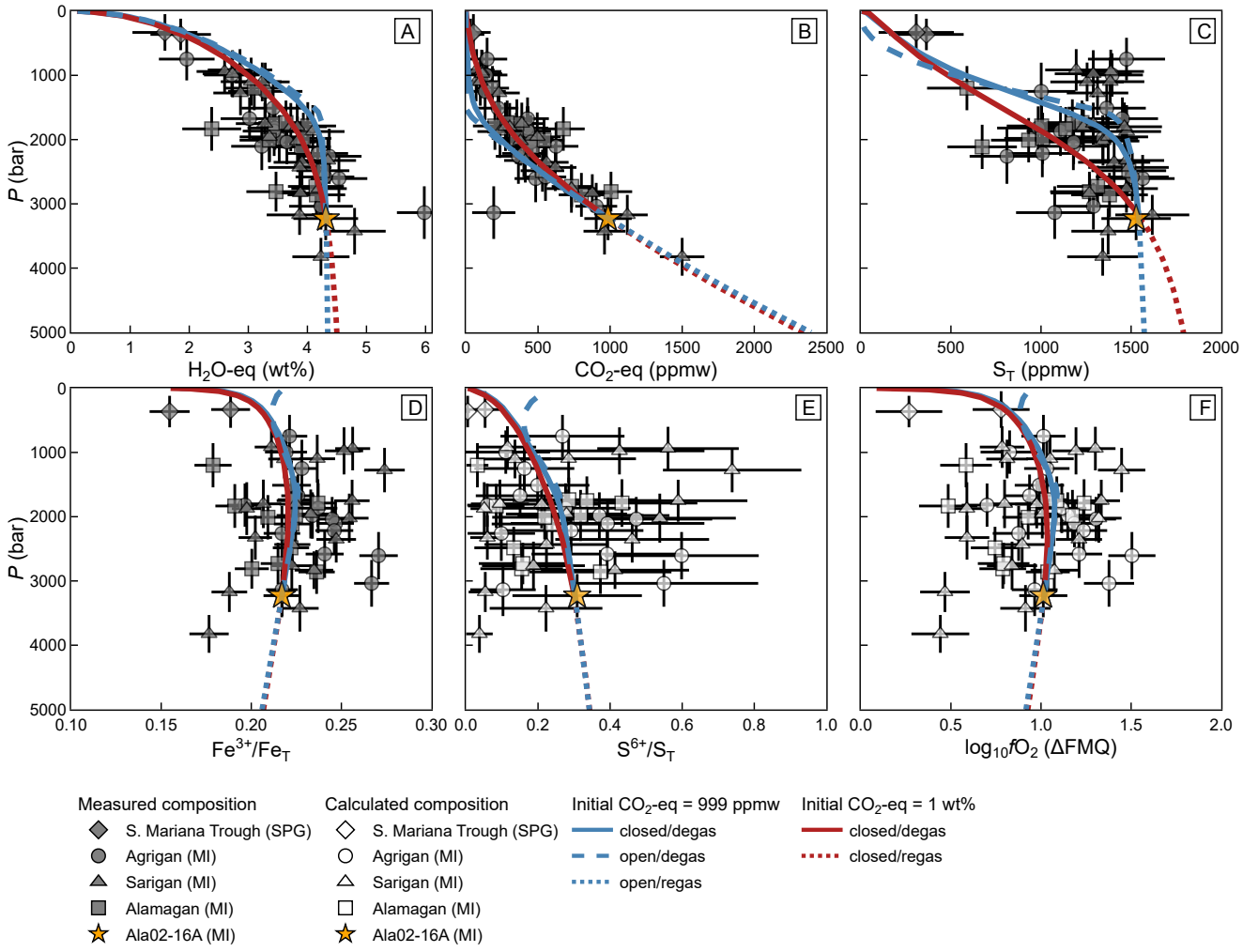

Figure 7: Melt composition for open- and closed-system re- and degassing calculations (Section 4.3) for Ala02-16A from the Marianas dataset, showing P vs. [A] H_2O-eq, [B] CO_2-eq, [C] S_T, [D] Fe^{3+}/Fe_T; [E] S^{6+}/S_T, and [F] ΔFMQ. Curves begin at melt inclusion Ala02-16A (yellow star) for: closed-system degassing assuming Ala02-16A represents the bulk composition of the system (blue solid); closed-system degassing (red solid) and regassing (red dot) assuming the bulk system contains 1 wt.% CO_2-eq; and open-system degassing (blue dash) and regassing (blue dot). Symbols show measured melt volatile contents (grey, [A]–[D]) or calculated values (white, [E] and [F]) at calculated P^v_{sat} (Section 4.1) for natural glasses for comparison with the degassing paths calculated using VolFe. The shape indicates MI or SPG and volcano (diamond = Southern Mariana Trough SPG, circle = Agrigan MI, square = Sarigan MI, and triangle = Alamagan MI). Error bars are 2 sigma based on measurement uncertainty or propagated uncertainty using a Monte Carlo approach.

5 Comparison to other approaches

As emphasised in Section 1, there are several other tools available to calculate melt-vapour chemical equilibria. These tools differ from VolFe in a variety of ways, including: the volatile components considered; the melt and vapour species considered; their approach to formulation; parameterisations of model-dependent variables available; and the types of calculations for which they are best suited. A full comparison of the various tools is beyond the scope of this paper (further discussion in Supplementary Material Section S5), so only key features are discussed here; a preliminary comparison between VolFe and other tools can also be found in Hughes et al. [2023a].

The tools we compare to here are VolatileCalc [Newman and Lowenstern 2002], VESIcal [Iacovino et al. 2021], Solwcad [Papale et al. 2006], MagmaSat [Ghiorso and Gualda 2015], SolEx [Witham et al. 2012], Sulfur_X [Ding et al. 2023], CHOSETTO [Moretti and Ottonello 2003; Moretti and Papale 2004], MELTS+DEW [Ghiorso et al. 2023], Petrolog4, D-Compress [Burgisser et al. 2015], EVo [Liggins et al. 2020; 2022], and MAGEC [Sun and Lee 2022; Sun and Yao 2024]. The key similarities and differences are outlined in Table 5 and the following bullet points.

- Modelling sulfur: SolEx, Sulfur_X, and Petrolog4 use a partition coefficient approach rather than the solubility function approach on which D-Compress, CHOSETTO, EVo, MAGEC, and VolFe are based.

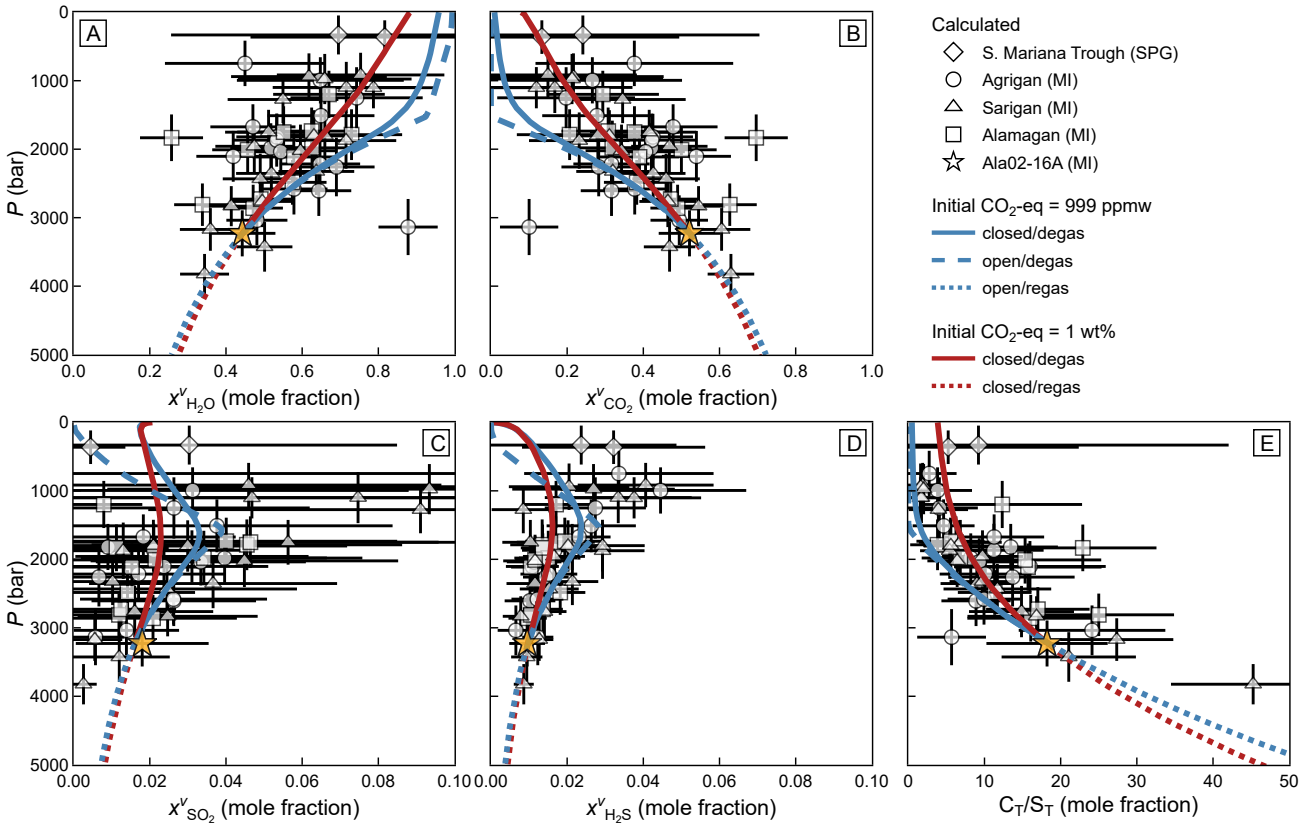

Figure 8: Vapour composition for open- and closed-system re- and degassing calculations (Section 4.3) for Ala02-16A from the Marianas dataset, showing P vs. mole fraction in the vapour for: [A] H_2O, [B] CO_2, [C] SO_2, [D] H_2S; and [E] C_T/S_T. All other vapour species (O_2, H_2, CO, S_2, CH_4, and OCS) are always <0.01 mole fraction. Curves begin at melt inclusion Ala02-16A (yellow star) for: closed-system degassing assuming Ala02-16A represents the bulk composition of the system (blue solid); closed-system degassing (red solid) and regassing (red dot) assuming the bulk system has 1 wt.% CO_2-eq; and open-system degassing (blue dash) and regassing (blue dot). Symbols (white) show calculated vapour speciation at calculated P^v_{sat} (Section 4.1) for natural glasses for comparison with the degassing paths calculated using `VolFe`. The shape indicates MI or SPG and volcano (diamond = Southern Mariana Trough SPG, circle = Agrigan MI, square = Sarigan MI, and triangle = Alamagan MI). Error bars are 2 sigma based on propagated uncertainty using a Monte Carlo approach.

• Oxygen: `Sulfur_X`, `D-Compress`, `Petrolog4`, `EVo`, `MAGEC`, and `VolFe` are a closed system with respect to oxygen during closed-system degassing. `CHOSETTO` externally buffers the system during degassing and hence oxygen is not conserved.

• Calculation types: All these tools calculate closed-system degassing paths. Some tools calculate open-system degassing (e.g. `VolatileCalc`). Only `VolFe` calculated open- and closed regassing. Most of the tools can calculate P^v_{sat} (except `CHOSETTO` and `D-Compress`). Some tools can calculate isobars (e.g. `VolatileCalc`, `VESIcal`, etc.). None aim to calculate melt-vapour composition for other independent variables (e.g. fO_2 from sulfur content), although `MIMiC` [Rasmussen et al. 2020] can do calculations along constant volume paths based on `VolatileCalc` and `Petrolog4` has T as a dependent variable.

• Model-dependent variables: A wide variety of parameterisations for model-dependent variables are employed across the range of tools, especially in their chosen functional forms and parameterisations of the solubility functions employed.

Overall, `VolFe` is most similar to `EVo` and `MAGEC` in terms of the species and reactions considered in the melt and vapour, but different parameterisations of model-dependent variables are available in the different tools. Results of closed-system degassing calculations assuming Ala02-16A represents the bulk composition of the system using `VESIcal` (Dixon model), `CHOSETTO`, `Sulfur_X`, and `EVo` are shown in Figure 3E–3F (inputs for these calculations and a Jupyter Notebook for the calculations can be found in the GitHub repository and ReadTheDocs). As observed by Ding et al. [2023] and Hughes et al. [2023a], these models produce different results due to a combination of the melt and vapour species considered, approach to formulation, and parameterisations of model-dependent variables used.

6 Future work

Our goal is to make `VolFe` a flexible and adaptable tool for predicting and understanding trends relating to melt-vapour equilibrium in natural magmas based on a thermodynamically consistent framework. However, the data underlying `VolFe` is

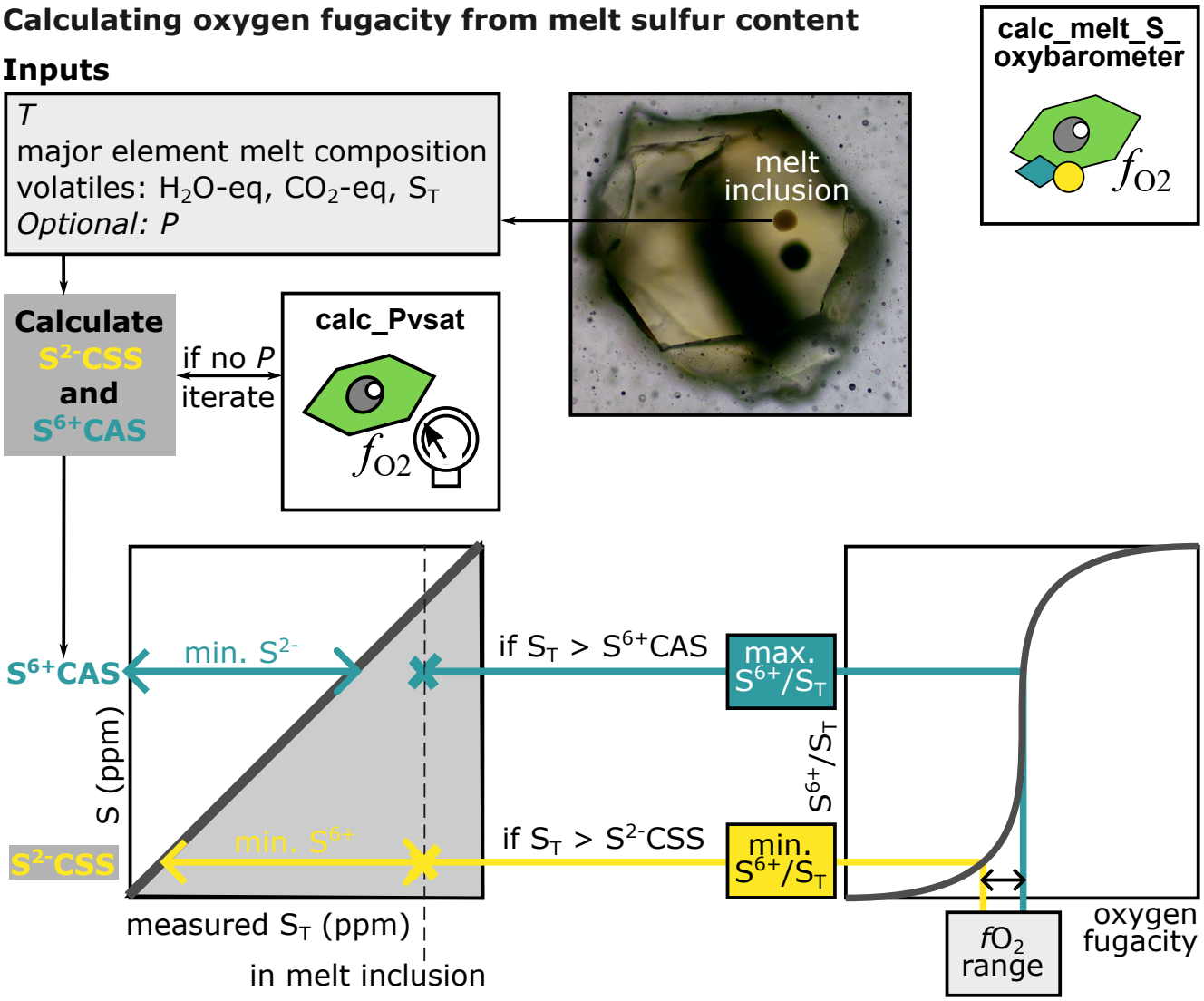

Figure 9: Schematic of how the melt sulfur content oxybarometer works. The crosses represent the measured S_T vs. calculated S^{2-}CSS and S^{6+}CAS.

a moving target. As we have tried to emphasise, an important feature is the ability to update `VolFe` by modifying it so as to include new thermochemical data (e.g. data on solubilities of various volatiles; fugacities and mixing relations of vapour species; etc.) and adding new user options (including other choices of independent variables and the paths they follow). Additionally, new calculation types can be incorporated as they become useful, as well as modifying the thermodynamic framework (e.g. new volatiles, species, phases) to enable more complex systems to be modelled. Continued improvement of interoperability with other relevant `Python` packages (e.g. `PySulfSat` [Wieser and Gleeson 2023]; `DensityX` [Iacovino and Till 2019]) is key to the continued improvement of geochemical modelling, as well as the evaluation and incorporation of uncertainties of model-dependent variables into calculations. A robust comparison with other melt-vapour chemical equilibria will also be crucial in enabling the community to understand the strengths and limitations of the different tools available.

7 Summary

We have described the thermodynamic framework and currently available calculation types for `VolFe`, an open-source `Python` package to calculate melt-vapour equilibria. `VolFe` considers a variety of both oxidised and reduced volatile-bearing species containing C, H, S, O, and noble gases such that it can be applied to terrestrial (e.g. MORB, arc, and ocean islands) and extra-terrestrial (e.g. Moon, Mars, and Io) systems. Various parameterisations of model dependent variables (e.g. fugacity coefficients, equilibrium constants for homogeneous vapour equilibria, solubility functions for heterogeneous melt-vapour equilibria, saturation conditions, etc.) enable modelling of basaltic through rhyolitic melts, with the hope that new parameterisations will be added as new studies are published. The main calculation types are the pressure of vapour-saturation and range in fO_2 based on the measured sulfur content from melt inclusion and matrix glass data; as well as open- and closed-system re- and degassing paths. We applied `VolFe` calculations to data from the Marianas arc to

Table 5: Some of the key similarities and differences between tools available to calculate melt-vapour chemical equilibria.

	VolatileCalc	VESIcal	Solwcad	MagmaSat	SolEx	Sulfur_X	CHOSETTO	MELTS+DEW	Petrolog4	D-Compress	EVo	MAGEC	VolFe
Water and CO_2 in the melt and vapour	✓	✓	✓	✓	✓	✓	✓	✓	✓	✓	✓	✓	✓
H_2, CO, and CH_4 in the melt and vapour	×	×	×	×	×	×	×	×	×	✓	✓	✓	✓
Sulfur-bearing species in the vapour	×	×	×	×	S_T	H_2S SO_2	H_2S SO_2	H_2S SO_2	H_2S SO_2	S_2 H_2S SO_2†	S_2 H_2S SO_2	S_2 H_2S SO_2 OCS	S_2 H_2S SO_2 OCS
Sulfur-bearing species in the melt	×	×	×	×	S_T	S^{2-} S^{6+}	S^{2-} S^{6+}	S^{2-} S^{6+}	S^{2-} S^{6+}	H_2S SO_2	S^{2-} S^{6+}	S^{2-} S^{6+}	*S^{2-} H_2S S^{6+}
Other species	×	×	×	×	Cl	×	×	Cl F	×	×	N_2	×	"X"

† D-Compress additionally considers OCS for gas species calculations at atmospheric pressure.

illustrate the types of results that can be calculated from melt inclusion and submarine pillow glass data.

Author Contributions

ECH and EMS conceived the project. ECH is the main developer of VolFe with support from PL and PW and input on direction from EMS. ECH wrote the first draft of the manuscript and all authors contributed to subsequent drafts.

Acknowledgements

We thank two anonymous reviewers and Meng Tian for their thorough and constructive comments, and Kayla Iacovino for their editorial handling and comments, that greatly improved both the manuscript and Python package. ECH was funded by a Caltech Geology Option Post-Doctoral Fellowship and a Caltech Centre for Comparative Planetary Evolution (^{3}CPE) research grant and was supported by the New Zealand Ministry of Business, Innovation and Employment (MBIE) through the Hazards and Risk Management (Strategic Science Investment Fund, contract C05X1702). PL acknowledges an Embiricos Trust scholarship from Jesus College, University of Cambridge. PW acknowledges funding from a Sloan Research Fellowship.

Data Availability

VolFe is freely available on GitHub (https://github.com/eryhughes/VolFe) and installable using PyPI (the version number should be stated for calculations used). There is documentation on ReadTheDocs (https://VolFe.readthedocs.io/en/latest/) and the code is archived in Zenodo [Hughes et al. 2025]. Code for deriving the differential equations used in the solver is available as a Jupyter Notebook in the GitHub repository. Jupyter Notebooks for the benchmarking calculations for model dependent variables, as well as comparisons to other tools for isobar and degassing calculations, are in the GitHub repository and ReadTheDocs. Additionally, Jupyter Notebooks for worked examples of all calculation types (including the Marianas example) are available in the GitHub repository and ReadTheDocs.

Copyright Notice

References

Aiuppa, A., M. Bitetto, S. Calabrese, D. Delle Donne, J. Lages, F. P. La Monica, G. Chiodini, G. Tamburello, A. Cotterill, P. Fulignati, A. Gioncada, E. J. Liu, R. Moretti, and M. Pistolesi (2022). "Mafic magma feeds degassing unrest at Vulcano Island, Italy". *Communications Earth & Environment* 3(1). DOI: 10.1038/s43247-022-00589-1.

Allison, C. M., K. Roggensack, and A. B. Clarke (2022). "MafiCH: a general model for H_2O–CO_2 solubility in mafic magmas". *Contributions to Mineralogy and Petrology* 177(3). DOI: 10.1007/s00410-022-01903-y.

Anderson, A. T. and T. L. Wright (1972). "Phenocrysts and glass inclusions and their bearing on oxidation and mixing of basaltic magmas, Kilauea volcano, Hawaii". *American Mineralogist: Journal of Earth and Planetary Materials* 57(1-2), pages 188–216.

Anderson Jr, A. T., S. Newman, S. N. Williams, T. H. Druitt, C. Skirius, and E. Stolper (1989). "H_2O, CO_2, Cl, and gas in Plinian and ash-flow Bishop rhyolite". *Geology*

17(3), pages 221–225. DOI: 10.1130/0091-7613(1989)017<0221:HOCCAG>2.3.CO;2.

Applegarth, L., H. Tuffen, M. James, and H. Pinkerton (2013). "Degassing-driven crystallisation in basalts". *Earth-Science Reviews* 116, pages 1–16. DOI: 10.1016/j.earscirev.2012.10.007.

Ardia, P., M. Hirschmann, A. Withers, and B. Stanley (2013). "Solubility of CH_4 in a synthetic basaltic melt, with applications to atmosphere–magma ocean–core partitioning of volatiles and to the evolution of the Martian atmosphere". *Geochimica et Cosmochimica Acta* 114, pages 52–71. DOI: 10.1016/j.gca.2013.03.028.

Armstrong, L. S., M. M. Hirschmann, B. D. Stanley, E. G. Falksen, and S. D. Jacobsen (2015). "Speciation and solubility of reduced C–O–H–N volatiles in mafic melt: Implications for volcanism, atmospheric evolution, and deep volatile cycles in the terrestrial planets". *Geochimica et Cosmochimica Acta* 171, pages 283–302. DOI: 10.1016/j.gca.2015.07.007.

Beermann, O., R. Botcharnikov, F. Holtz, O. Diedrich, and M. Nowak (2011). "Temperature dependence of sulfide and sulfate solubility in olivine-saturated basaltic magmas". *Geochimica et Cosmochimica Acta* 75(23), pages 7612–7631. DOI: 10.1016/j.gca.2011.09.024.

Behrens, H., S. Ohlhorst, F. Holtz, and M. Champenois (2004). "CO_2 solubility in dacitic melts equilibrated with H_2O-CO_2 fluids: Implications for modeling the solubility of CO_2 in silicic melts". *Geochimica et Cosmochimica Acta* 68(22), pages 4687–4703. DOI: 10.1016/j.gca.2004.04.019.

Belgrano, T. M., P. M. Tollan, F. Marxer, and L. W. Diamond (2021). "Paleobathymetry of Submarine Lavas in the Samail and Troodos Ophiolites: Insights From Volatiles in Glasses and Implications for Hydrothermal Systems". *Journal of Geophysical Research: Solid Earth* 126(7). DOI: 10.1029/2021jb021966.

Belonoshko, A. and S. Saxena (1992). "A unified equation of state for fluids of C-H-O-N-S-Ar composition and their mixtures up to very high temperatures and pressures". *Geochimica et Cosmochimica Acta* 56(10), pages 3611–3626. DOI: 10.1016/0016-7037(92)90157-e.

Black, B. A. and B. J. Andrews (2020). "Petrologic imaging of the architecture of magma reservoirs feeding caldera-forming eruptions". *Earth and Planetary Science Letters* 552, page 116572. DOI: 10.1016/j.epsl.2020.116572.

Blank, J. G. and R. A. Brooker (1994). "Experimental studies of carbon dioxide in silicate melts; solubility, speciation, and stable carbon isotope behavior". *Reviews in Mineralogy and Geochemistry* 30(1), pages 157–186.

Blank, J. G., E. M. Stolper, and M. R. Carroll (1993). "Solubilities of carbon dioxide and water in rhyolitic melt at 850°C and 750 bars". *Earth and Planetary Science Letters* 119(1–2), pages 27–36. DOI: 10.1016/0012-821x(93)90004-s.

Blundy, J. and K. Cashman (2008). "Petrologic Reconstruction of Magmatic System Variables and Processes". *Reviews in Mineralogy and Geochemistry* 69(1), pages 179–239. DOI: 10.2138/rmg.2008.69.6.

Borisov, A., H. Behrens, and F. Holtz (2018). "Ferric/ferrous ratio in silicate melts: a new model for 1 atm data with special emphasis on the effects of melt composition". *Contributions to Mineralogy and Petrology* 173(12). DOI: 10.1007/s00410-018-1524-8.

Botcharnikov, R., H. Behrens, and F. Holtz (2006). "Solubility and speciation of C–O–H fluids in andesitic melt at T=1100–1300°C and P=200 and 500MPa". *Chemical Geology* 229(1–3), pages 125–143. DOI: 10.1016/j.chemgeo.2006.01.016.

Boulliung, J. and B. J. Wood (2022). "SO_2 solubility and degassing behavior in silicate melts". *Geochimica et Cosmochimica Acta* 336, pages 150–164. DOI: 10.1016/j.gca.2022.08.032.

– (2023a). "Corrigendum to "SO_2 solubility and degassing behavior in silicate melts" [Geochim. Cosmochim. Acta 336 (2022) 150–164]". *Geochimica et Cosmochimica Acta* 343, page 420. DOI: 10.1016/j.gca.2022.11.025.

– (2023b). "Sulfur oxidation state and solubility in silicate melts". *Contributions to Mineralogy and Petrology* 178(8). DOI: 10.1007/s00410-023-02033-9.

Brooker, R., S. Kohn, J. Holloway, P. McMillan, and M. Carroll (1999). "Solubility, speciation and dissolution mechanisms for CO_2 in melts on the $NaAlO_2$–SiO_2 join". *Geochimica et Cosmochimica Acta* 63(21), pages 3549–3565. DOI: 10.1016/s0016-7037(99)00196-9.

Brounce, M. N., K. A. Kelley, and E. Cottrell (2014). "Variations in $Fe^{3+}/\sum Fe$ of Mariana Arc Basalts and Mantle Wedge fO_2". *Journal of Petrology* 55(12), pages 2513–2536. DOI: 10.1093/petrology/egu065.

Brounce, M. N., E. Stolper, and J. Eiler (2017). "Redox variations in Mauna Kea lavas, the oxygen fugacity of the Hawaiian plume, and the role of volcanic gases in Earth's oxygenation". *Proceedings of the National Academy of Sciences* 114(34), pages 8997–9002. DOI: 10.1073/pnas.1619527114.

Burgisser, A., M. Alletti, and B. Scaillet (2015). "Simulating the behavior of volatiles belonging to the C–O–H–S system in silicate melts under magmatic conditions with the software D-Compress". *Computers & Geosciences* 79, pages 1–14. DOI: 10.1016/j.cageo.2015.03.002.

Burgisser, A. and B. Scaillet (2007). "Redox evolution of a degassing magma rising to the surface". *Nature* 445(7124), pages 194–197. DOI: 10.1038/nature05509.

Burnham, C. W. (1979). "Importance of volatile constituents". *https://www.jstor.org/stable/j.ctt13x1dkm*. Edited by H. S. Yoder Jr. Princeton: Princeton University Press.

Burnham, C. W. and N. F. Davis (1974). "The role of H_2O in silicate melts; II, Thermodynamic and phase relations in the system $NaAlSi_3O_8$—H_2O to 10 kilobars, 700 degrees to 1100 degrees C". *American Journal of Science* 274(8), pages 902–940. DOI: 10.2475/ajs.274.8.902.

Burton, M., A. Aiuppa, P. Allard, M. Asensio-Ramos, A. P. Cofrades, A. La Spina, E. J. Nicholson, V. Zanon, J. Barrancos, M. Bitetto, M. Hartley, J. E. Romero, E. Waters, A. Stewart, P. A. Hernández, J. P. Lages, E. Padrón, K. Wood, B. Esse, C. Hayer, K. Cyrzan, E. F. Rose-Koga, F. Schiavi, L. D'Auria, and N. M. Pérez (2023). "Exceptional eruptive CO_2 emissions from intra-plate alkaline magmatism in the Canary volcanic archipelago". *Communications Earth & Environment* 4(1). DOI: 10.1038/s43247-023-01103-x.

Camejo-Harry, M., E. Melekhova, J. Blundy, W. Attridge, R. Robertson, and T. Christopher (2018). "Magma evolution beneath Bequia, Lesser Antilles, deduced from petrology of lavas and plutonic xenoliths". *Contributions to Mineralogy and Petrology* 173(10). DOI: 10.1007/s00410-018-1504-z.

Camejo-Harry, M., E. Melekhova, J. Blundy, and R. Robertson (2019). "Evolution in magma storage conditions beneath Kick-'em-Jenny and Kick-'em-Jack submarine volcanoes, Lesser Antilles arc". *Journal of Volcanology and Geothermal Research* 373, pages 1–22. DOI: 10.1016/j.jvolgeores.2019.01.023.

Candela, P. A. (1986). "The evolution of aqueous vapor from silicate melts: Effect on oxygen fugacity". *Geochimica et Cosmochimica Acta* 50(6), pages 1205–1211. DOI: 10.1016/0016-7037(86)90403-5.

Carey, R. J., M. Manga, W. Degruyter, H. Gonnermann, D. Swanson, B. Houghton, T. Orr, and M. Patrick (2013). "Convection in a volcanic conduit recorded by bubbles". *Geology* 41(4), pages 395–398. DOI: 10.1130/g33685.1.

Carmichael, I. S. E. and M. S. Ghiorso (1986). "Oxidation-reduction relations in basic magma: a case for homogeneous equilibria". *Earth and Planetary Science Letters* 78(2–3), pages 200–210. DOI: 10.1016/0012-821x(86)90061-0.

– (1990). "The effect of oxygen fugacity on the redox state of natural liquids and their crystallizing phases". *Reviews in Mineralogy and Geochemistry* 24(1), pages 191–212.

Chowdhury, P. and R. Dasgupta (2019). "Effect of sulfate on the basaltic liquidus and Sulfur Concentration at Anhydrite Saturation (SCAS) of hydrous basalts – Implications for sulfur cycle in subduction zones". *Chemical Geology* 522, pages 162–174. DOI: 10.1016/j.chemgeo.2019.05.020.

Colman, A., J. M. Sinton, and V. D. Wanless (2015). "Constraints from melt inclusions on depths of magma residence at intermediate magma supply along the Galápagos Spreading Center". *Earth and Planetary Science Letters* 412, pages 122–131. DOI: 10.1016/j.epsl.2014.12.007.

Coombs, M. L., T. W. Sisson, and P. W. Lipman (2006). "Growth history of Kilauea inferred from volatile concentrations in submarine-collected basalts". *Journal of Volcanology and Geothermal Research* 151(1–3), pages 19–49. DOI: 10.1016/j.jvolgeores.2005.07.037.

Cottrell, E., S. K. Birner, M. Brounce, F. A. Davis, L. E. Waters, and K. A. Kelley (2021). "Oxygen Fugacity Across Tectonic Settings". *Magma Redox Geochemistry*, pages 33–61. DOI: 10.1002/9781119473206.ch3.

Denbigh, K. G. (1981). *The principles of chemical equilibrium: with applications in chemistry and chemical engineering*. 3rd edition. Cambridge, UK: Cambridge University Press. ISBN: 978-0521096553.

Ding, S., T. Plank, P. J. Wallace, and D. J. Rasmussen (2023). "Sulfur_X: A Model of Sulfur Degassing During Magma Ascent". *Geochemistry, Geophysics, Geosystems* 24(4). DOI: 10.1029/2022gc010552.

Dingwell, D. B., C. Romano, and K.-U. Hess (1996). "The effect of water on the viscosity of a haplogranitic melt under P-T-X conditions relevant to silicic volcanism". *Contributions to Mineralogy and Petrology* 124(1), pages 19–28. DOI: 10.1007/s004100050170.

Dixon, J. E. (1997). "Degassing of alkalic basalts". *American Mineralogist* 82(3–4), pages 368–378. DOI: 10.2138/am-1997-3-415.

Dixon, J. E. and E. M. Stolper (1995). "An experimental study of water and carbon dioxide solubilities in mid-ocean ridge basaltic liquids. Part II: applications to degassing". *Journal of petrology* 36(6), pages 1633–1646. DOI: 10.1093/oxfordjournals.petrology.a037268.

Dixon, J. E., E. M. Stolper, and J. R. Holloway (1995). "An experimental study of water and carbon dioxide solubilities in mid-ocean ridge basaltic liquids. Part I: calibration and solubility models". *Journal of Petrology* 36(6), pages 1607–1631. DOI: 10.1093/oxfordjournals.petrology.a037267.

Fincham, C. J. B. and F. D. Richardson (1954). "The behaviour of sulphur in silicate and aluminate melts". *Proceedings of the Royal Society of London. Series A. Mathematical and Physical Sciences* 223(1152), pages 40–62. DOI: 10.1098/rspa.1954.0099.

Fine, G. and E. Stolper (1985). "The speciation of carbon dioxide in sodium aluminosilicate glasses". *Contributions to Mineralogy and Petrology* 91(2), pages 105–121. DOI: 10.1007/bf00377759.

– (1986). "Dissolved carbon dioxide in basaltic glasses: concentrations and speciation". *Earth and Planetary Science Letters* 76(3–4), pages 263–278. DOI: 10.1016/0012-821x(86)90078-6.

Flowers, G. C. (1979). "Correction of Holloway's (1977) adaptation of the modified Redlich-Kwong equation of state for calculation of the fugacities of molecular species in supercritical fluids of geologic interest". *Contributions to Mineralogy and Petrology* 69(3), pages 315–318. DOI: 10.1007/bf00372333.

Fortin, M.-A., J. Riddle, Y. Desjardins-Langlais, and D. R. Baker (2015). "The effect of water on the sulfur concentration at sulfide saturation (SCSS) in natural melts". *Geochimica et Cosmochimica Acta* 160, pages 100–116. DOI: 10.1016/j.gca.2015.03.022.

Frost, B. R. (1991). "Introduction to oxygen fugacity and its petrologic importance". *Oxide minerals: Petrologic and Magnetic Significance*. Edited by D. H. Lindsley. Volume 25. De Gruyter, pages 1–10.

Gaillard, F. and B. Scaillet (2014). "A theoretical framework for volcanic degassing chemistry in a comparative planetology perspective and implications for planetary atmospheres". *Earth and Planetary Science Letters* 403, pages 307–316. DOI: 10.1016/j.epsl.2014.07.009.

Gaillard, F., B. Scaillet, and N. T. Arndt (2011). "Atmospheric oxygenation caused by a change in volcanic degassing pressure". *Nature* 478(7368), pages 229–232. DOI: 10.1038/nature10460.

Gaillard, F., B. Scaillet, M. Pichavant, and G. Iacono-Marziano (2015). "The redox geodynamics linking basalts and their mantle sources through space and time". *Chemical Geology* 418, pages 217–233. DOI: 10.1016/j.chemgeo.2015.07.030.

Ghiorso, M. S., S. Matthews, and D. Sverjensky (2023). "MELTS+DEW: Modeling major element+Cl+F+S phase equilibria, redox reactions and elemental partitioning in

magmatic-hydrothermal systems". *Goldschmidt abstracts*. Conference Proceedings. Goldschmidt. Lyon, France: European Association of Geochemistry and the Geochemical Society.

Ghiorso, M. S. and G. A. R. Gualda (2015). "An H_2O–CO_2 mixed fluid saturation model compatible with rhyolite-MELTS". *Contributions to Mineralogy and Petrology* 169(6). DOI: 10.1007/s00410-015-1141-8.

Gibbs, J. W. (1876). "On the equilibrium of heterogeneous substances". *American journal of science* 3(96), pages 108–248.

– (1878). "On the equilibrium of heterogeneous substances". *American journal of science* 3(96), pages 343–524.

Hartley, M. E., J. Maclennan, M. Edmonds, and T. Thordarson (2014). "Reconstructing the deep CO_2 degassing behaviour of large basaltic fissure eruptions". *Earth and Planetary Science Letters* 393, pages 120–131. DOI: 10.1016/j.epsl.2014.02.031.

Hirschmann, M. M., A. C. Withers, P. Ardia, and N. T. Foley (2012). "Solubility of molecular hydrogen in silicate melts and consequences for volatile evolution of terrestrial planets". *Earth and Planetary Science Letters* 345–348, pages 38–48. DOI: 10.1016/j.epsl.2012.06.031.

Holland, T. and R. Powell (1991). "A Compensated-Redlich-Kwong (CORK) equation for volumes and fugacities of CO_2 and H_2O in the range 1 bar to 50 kbar and 100–1600 °C". *Contributions to Mineralogy and Petrology* 109(2), pages 265–273. DOI: 10.1007/bf00306484.

Holloway, J. R. and J. G. Blank (1994). "Application of experimental results to COH species in natural melts". *Reviews in Mineralogy and Geochemistry* 30(1), pages 187–230.

Holloway, J. R., V. Pan, and G. Gudmundsson (1992). "High-pressure fluid-absent melting experiments in the presence of graphite: oxygen fugacity, ferric/ferrous ratio and dissolved CO_2". *European Journal of Mineralogy* 4(1), pages 105–114.

Holloway, J. R. (1977). "Fugacity and Activity of Molecular Species in Supercritical Fluids". *Thermodynamics in Geology*. Springer Netherlands, pages 161–181. ISBN: 9789401012522. DOI: 10.1007/978-94-010-1252-2_9.

Hughes, E. C., S. Ding, K. Iacovino, P. Wieser, and G. Kilgour (2023a). "Workshop report: Modelling volatile behaviour in magmas". *EarthArXiv*. DOI: 10.31223/x5fd3q. [Preprint].

Hughes, E. C., P. Liggins, L. Saper, and E. M. Stolper (2024). "The effects of oxygen fugacity and sulfur on the pressure of vapor-saturation of magma". *American Mineralogist* 109(3), pages 422–438. DOI: 10.2138/am-2022-8739.

Hughes, E. C., P. Liggins, and P. Wieser (2025). "eryhughes/VolFe: VolFe". *Zenodo*. DOI: 10.5281/ZENODO.15756762. [Software].

Hughes, E. C., L. M. Saper, P. Liggins, H. S. C. O'Neill, and E. M. Stolper (2023b). "The sulfur solubility minimum and maximum in silicate melt". *Journal of the Geological Society* 180(3). DOI: 10.1144/jgs2021-125.

Iacono-Marziano, G., Y. Morizet, E. Le Trong, and F. Gaillard (2012). "New experimental data and semi-empirical parameterization of H_2O–CO_2 solubility in mafic melts". *Geochimica et Cosmochimica Acta* 97, pages 1–23. DOI: 10.1016/j.gca.2012.08.035.

Iacono-Marziano, G., A. Paonita, A. Rizzo, B. Scaillet, and F. Gaillard (2010). "Noble gas solubilities in silicate melts: New experimental results and a comprehensive model of the effects of liquid composition, temperature and pressure". *Chemical Geology* 279(3–4), pages 145–157. DOI: 10.1016/j.chemgeo.2010.10.017.

Iacovino, K. (2015). "Linking subsurface to surface degassing at active volcanoes: A thermodynamic model with applications to Erebus volcano". *Earth and Planetary Science Letters* 431, pages 59–74. DOI: 10.1016/j.epsl.2015.09.016.

Iacovino, K., S. Matthews, P. E. Wieser, G. M. Moore, and F. Bégué (2021). "VESIcal Part I: An Open-Source Thermodynamic Model Engine for Mixed Volatile (H_2O-CO_2) Solubility in Silicate Melts". *Earth and Space Science* 8(11). DOI: 10.1029/2020ea001584.

Iacovino, K. and C. B. Till (2019). "DensityX: A program for calculating the densities of magmatic liquids up to 1,627 °C and 30 kbar". *Volcanica* 2(1), pages 1–10. DOI: 10.30909/vol.02.01.0110.

Kadik, A. A., O. A. Lukanin, Y. B. Lebedev, and E. Y. Korovushkina (1972). "Solubility of H_2O and CO_2 in granite and basalt melts at high pressures". *Geochemistry International* 9, pages 1041–1050.

Kelley, K. A. and E. Cottrell (2012). "The influence of magmatic differentiation on the oxidation state of Fe in a basaltic arc magma". *Earth and Planetary Science Letters* 329–330, pages 109–121. DOI: 10.1016/j.epsl.2012.02.010.

King, P. and J. Holloway (2002). "CO_2 solubility and speciation in intermediate (andesitic) melts: the role of H_2O and composition". *Geochimica et Cosmochimica Acta* 66(9), pages 1627–1640. DOI: 10.1016/s0016-7037(01)00872-9.

Kolzenburg, S., D. Di Genova, D. Giordano, K. Hess, and D. Dingwell (2018). "The effect of oxygen fugacity on the rheological evolution of crystallizing basaltic melts". *Earth and Planetary Science Letters* 487, pages 21–32. DOI: 10.1016/j.epsl.2018.01.023.

Kress, V. C. and I. S. E. Carmichael (1991). "The compressibility of silicate liquids containing Fe_2O_3 and the effect of composition, temperature, oxygen fugacity and pressure on their redox states". *Contributions to Mineralogy and Petrology* 108(1–2), pages 82–92. DOI: 10.1007/bf00307328.

Lesne, P., B. Scaillet, and M. Pichavant (2015). "The solubility of sulfur in hydrous basaltic melts". *Chemical Geology* 418, pages 104–116. DOI: 10.1016/j.chemgeo.2015.03.025.

Lesne, P., B. Scaillet, M. Pichavant, and J.-M. Beny (2011a). "The carbon dioxide solubility in alkali basalts: an experimental study". *Contributions to Mineralogy and Petrology* 162(1), pages 153–168. DOI: 10.1007/s00410-010-0585-0.

Lesne, P., B. Scaillet, M. Pichavant, G. Iacono-Marziano, and J.-M. Beny (2011b). "The H_2O solubility of alkali basaltic melts: an experimental study". *Contributions to Mineralogy and Petrology* 162(1), pages 133–151. DOI: 10.1007/s00410-010-0588-x.

Liggins, P., S. Jordan, P. B. Rimmer, and O. Shorttle (2022). "Growth and Evolution of Secondary Volcanic Atmospheres: I. Identifying the Geological Character of Hot

Rocky Planets". *Journal of Geophysical Research: Planets* 127(7). DOI: 10.1029/2021je007123.

Liggins, P., O. Shorttle, and P. B. Rimmer (2020). "Can volcanism build hydrogen-rich early atmospheres?" *Earth and Planetary Science Letters* 550, page 116546. DOI: 10.1016/j.epsl.2020.116546.

Liu, K., L. Zhang, X. Guo, and H. Ni (2021). "Effects of sulfide composition and melt H_2O on sulfur content at sulfide saturation in basaltic melts". *Chemical Geology* 559, page 119913. DOI: 10.1016/j.chemgeo.2020.119913.

Liu, Y., N.-T. Samaha, and D. R. Baker (2007). "Sulfur concentration at sulfide saturation (SCSS) in magmatic silicate melts". *Geochimica et Cosmochimica Acta* 71(7), pages 1783–1799. DOI: 10.1016/j.gca.2007.01.004.

Lund, D. C., E. I. Seeley, P. D. Asimow, M. J. Lewis, S. E. McCart, and A. A. Mudahy (2018). "Anomalous Pacific-Antarctic Ridge Volcanism Precedes Glacial Termination 2". *Geochemistry, Geophysics, Geosystems* 19(8), pages 2478–2491. DOI: 10.1029/2017gc007341.

Macpherson, C. and D. Mattey (1994). "Carbon isotope variations of CO_2 in Central Lau Basin basalts and ferrobasalts". *Earth and Planetary Science Letters* 121(3–4), pages 263–276. DOI: 10.1016/0012-821x(94)90072-8.

Marshall, L. R., E. C. Maters, A. Schmidt, C. Timmreck, A. Robock, and M. Toohey (2022). "Volcanic effects on climate: recent advances and future avenues". *Bulletin of Volcanology* 84(5). DOI: 10.1007/s00445-022-01559-3.

Métrich, N., A. J. Berry, H. S. O'Neill, and J. Susini (2009). "The oxidation state of sulfur in synthetic and natural glasses determined by X-ray absorption spectroscopy". *Geochimica et Cosmochimica Acta* 73(8), pages 2382–2399. DOI: 10.1016/j.gca.2009.01.025.

Meurer, A., C. P. Smith, M. Paprocki, O. Čertík, S. B. Kirpichev, M. Rocklin, A. Kumar, S. Ivanov, J. K. Moore, S. Singh, T. Rathnayake, S. Vig, B. E. Granger, R. P. Muller, F. Bonazzi, H. Gupta, S. Vats, F. Johansson, F. Pedregosa, M. J. Curry, A. R. Terrel, Š. Roučka, A. Saboo, I. Fernando, S. Kulal, R. Cimrman, and A. Scopatz (2017). "SymPy: symbolic computing in Python". *PeerJ Computer Science* 3, e103. DOI: 10.7717/peerj-cs.103.

Moore, G., T. Vennemann, and I. S. E. Carmichael (1998). "An empirical model for the solubility of H_2O in magmas to 3 kilobars". *American Mineralogist* 83(1–2), pages 36–42. DOI: 10.2138/am-1998-1-203.

Moore, J. G., D. J. Fornari, and D. A. Clague (1985). "Basalts from the 1877 submarine eruption of Mauna Loa, Hawaii; new data on the variation of palagonitization rate with temperature". *U.S. Geological Survey Bulletin* (1663). DOI: 10.3133/b1663.

Moore, L. R., E. Gazel, R. Tuohy, A. S. Lloyd, R. Esposito, M. Steele-MacInnis, E. H. Hauri, P. J. Wallace, T. Plank, and R. J. Bodnar (2015). "Bubbles matter: An assessment of the contribution of vapor bubbles to melt inclusion volatile budgets". *American Mineralogist* 100(4), pages 806–823. DOI: 10.2138/am-2015-5036.

Moore, L. R. and R. J. Bodnar (2019). "A pedagogical approach to estimating the CO_2 budget of magmas". *Journal of the Geological Society* 176(2), pages 398–407. DOI: 10.1144/jgs2018-094.

Moretti, R. and G. Ottonello (2003). "Polymerization and disproportionation of iron and sulfur in silicate melts: insights from an optical basicity-based approach". *Journal of Non-Crystalline Solids* 323(1–3), pages 111–119. DOI: 10.1016/s0022-3093(03)00297-7.

Moretti, R. and P. Papale (2004). "On the oxidation state and volatile behavior in multicomponent gas–melt equilibria". *Chemical Geology* 213(1–3), pages 265–280. DOI: 10.1016/j.chemgeo.2004.08.048.

Moune, S., F. Holtz, and R. E. Botcharnikov (2009). "Sulphur solubility in andesitic to basaltic melts: implications for Hekla volcano". *Contributions to Mineralogy and Petrology* 157(6), pages 691–707. DOI: 10.1007/s00410-008-0359-0.

Moussallam, Y., M. Edmonds, B. Scaillet, N. Peters, E. Gennaro, I. Sides, and C. Oppenheimer (2016). "The impact of degassing on the oxidation state of basaltic magmas: A case study of Kīlauea volcano". *Earth and Planetary Science Letters* 450, pages 317–325. DOI: 10.1016/j.epsl.2016.06.031.

Moussallam, Y., C. Oppenheimer, and B. Scaillet (2019). "On the relationship between oxidation state and temperature of volcanic gas emissions". *Earth and Planetary Science Letters* 520, pages 260–267. DOI: 10.1016/j.epsl.2019.05.036.

Moussallam, Y., C. Oppenheimer, B. Scaillet, F. Gaillard, P. Kyle, N. Peters, M. Hartley, K. Berlo, and A. Donovan (2014). "Tracking the changing oxidation state of Erebus magmas, from mantle to surface, driven by magma ascent and degassing". *Earth and Planetary Science Letters* 393, pages 200–209. DOI: 10.1016/j.epsl.2014.02.055.

Muth, M. J. and P. J. Wallace (2022). "Sulfur recycling in subduction zones and the oxygen fugacity of mafic arc magmas". *Earth and Planetary Science Letters* 599, page 117836. DOI: 10.1016/j.epsl.2022.117836.

Mysen, B. O., D. Virgo, W. J. Harrison, and C. M. Scarfe (1980). "Solubility mechanisms of H_2O in silicate melts at high pressures and temperatures: a Raman spectroscopic study". *American Mineralogist* 65(9-10), pages 900–914.

Newman, S. and J. B. Lowenstern (2002). "VolatileCalc: a silicate melt–H_2O–CO_2 solution model written in Visual Basic for excel". *Computers & Geosciences* 28(5), pages 597–604. DOI: 10.1016/s0098-3004(01)00081-4.

O'Neill, H. S. C. (1987). "Quartz-fayalite-iron and quartz-fayalite-magnetite equilibria and the free energy of formation of fayalite (Fe_2SiO_4) and magnetite (Fe_3O_4)". *American Mineralogist* 72(1-2), pages 67–75.

– (2021). "The Thermodynamic Controls on Sulfide Saturation in Silicate Melts with Application to Ocean Floor Basalts". *Magma Redox Geochemistry*, pages 177–213. DOI: 10.1002/9781119473206.ch10.

O'Neill, H. S. C., A. J. Berry, and G. Mallmann (2018). "The oxidation state of iron in Mid-Ocean Ridge Basaltic (MORB) glasses: Implications for their petrogenesis and oxygen fugacities". *Earth and Planetary Science Letters* 504, pages 152–162. DOI: 10.1016/j.epsl.2018.10.002.

O'Neill, H. S. C. and J. A. Mavrogenes (2022). "The sulfate capacities of silicate melts". *Geochimica et Cosmochimica Acta* 334, pages 368–382. DOI: 10.1016/j.gca.2022.06.020.

Ohmoto, H. and D. M. Kerrick (1977). "Devolatilization equilibria in graphitic systems". *American Journal of Science* 277(8), pages 1013–1044. DOI: 10.2475/ajs.277.8.1013.

Papale, P., R. Moretti, and D. Barbato (2006). "The compositional dependence of the saturation surface of H_2O+CO_2 fluids in silicate melts". *Chemical Geology* 229(1–3), pages 78–95. DOI: 10.1016/j.chemgeo.2006.01.013.

Papale, P., R. Moretti, and A. Paonita (2022). "Thermodynamics of Multi-component Gas–Melt Equilibrium in Magmas: Theory, Models, and Applications". *Reviews in Mineralogy and Geochemistry* 87(1), pages 431–556. DOI: 10.2138/rmg.2022.87.10.

Powell, R., T. Holland, and B. Worley (1998). "Calculating phase diagrams involving solid solutions via non-linear equations, with examples using THERMOCALC". *Journal of Metamorphic Geology* 16(4), pages 577–588. DOI: 10.1111/j.1525-1314.1998.00157.x.

Prigogine, I. and R. Defay (1954). *Treatise on Thermodynamics Based on the Methods of Gibbs and De Donder*. London: Longmans, Green.

Putirka, K. D. (2008). "Thermometers and Barometers for Volcanic Systems". *Reviews in Mineralogy and Geochemistry* 69(1), pages 61–120. DOI: 10.2138/rmg.2008.69.3.

Ranta, E., S. A. Halldórsson, B. A. Óladóttir, M. A. Pfeffer, A. Caracciolo, E. Bali, G. H. Guðfinnsson, M. Kahl, and S. Barsotti (2024). "Magmatic Controls on Volcanic Sulfur Emissions at the Iceland Hotspot". *Geochemistry, Geophysics, Geosystems* 25(5). DOI: 10.1029/2024gc011443.

Rasmussen, D. J., T. A. Plank, P. J. Wallace, M. E. Newcombe, and J. B. Lowenstern (2020). "Vapor-bubble growth in olivine-hosted melt inclusions". *American Mineralogist* 105(12), pages 1898–1919. DOI: 10.2138/am-2020-7377.

Rose-Koga, E. F., A.-S. Bouvier, G. A. Gaetani, P. J. Wallace, C. M. Allison, J. A. Andrys, C. A. Angeles de la Torre, A. Barth, R. J. Bodnar, A. J. J. Bracco Gartner, D. Butters, A. Castillejo, B. Chilson-Parks, B. R. Choudhary, N. Cluzel, M. Cole, E. Cottrell, A. Daly, L. V. Danyushevsky, C. L. DeVitre, M. J. Drignon, L. France, M. Gaborieau, M. O. Garcia, E. Gatti, F. S. Genske, M. E. Hartley, E. C. Hughes, A. A. Iveson, E. R. Johnson, M. Jones, T. Kagoshima, Y. Katzir, M. Kawaguchi, T. Kawamoto, K. A. Kelley, J. M. Koornneef, M. D. Kurz, M. Laubier, G. D. Layne, A. Lerner, K.-Y. Lin, P.-P. Liu, A. Lorenzo-Merino, N. Luciani, N. Magalhães, H. R. Marschall, P. J. Michael, B. D. Monteleone, L. R. Moore, Y. Moussallam, M. Muth, M. L. Myers, D. F. Narváez, O. Navon, M. E. Newcombe, A. R. L. Nichols, R. L. Nielsen, A. Pamukcu, T. Plank, D. J. Rasmussen, J. Roberge, F. Schiavi, D. Schwartz, K. Shimizu, K. Shimizu, N. Shimizu, J. B. Thomas, G. T. Thompson, J. M. Tucker, G. Ustunisik, C. Waelkens, Y. Zhang, and T. Zhou (2021). "Silicate melt inclusions in the new millennium: A review of recommended practices for preparation, analysis, and data presentation". *Chemical Geology* 570, page 120145. DOI: 10.1016/j.chemgeo.2021.120145.

Sack, R. O., I. S. E. Carmichael, M. Rivers, and M. S. Ghiorso (1981). "Ferric-ferrous equilibria in natural silicate liquids at 1 bar". *Contributions to Mineralogy and Petrology* 75(4), pages 369–376. DOI: 10.1007/bf00374720.

Seaman, C., S. B. Sherman, M. O. Garcia, M. B. Baker, B. Balta, and E. Stolper (2004). "Volatiles in glasses from the HSDP2 drill core". *Geochemistry, Geophysics, Geosystems* 5(9). DOI: 10.1029/2003gc000596.

Shaw, H. R. and D. R. Wones (1964). "Fugacity coefficients for hydrogen gas between O degrees and 1000 degrees C, for pressures to 3000 atm". *American Journal of Science* 262(7), pages 918–929. DOI: 10.2475/ajs.262.7.918.

Shi, P. and S. Saxena (1992). "Thermodynamic modeing of the CHOS fluid system". *American Mineralogist* 77(9-10), pages 1038–1049.

Shishkina, T. A., R. E. Botcharnikov, F. Holtz, R. R. Almeev, A. M. Jazwa, and A. A. Jakubiak (2014). "Compositional and pressure effects on the solubility of H_2O and CO_2 in mafic melts". *Chemical Geology* 388, pages 112–129. DOI: 10.1016/j.chemgeo.2014.09.001.

Silver, L. A., P. D. Ihinger, and E. Stolper (1990). "The influence of bulk composition on the speciation of water in silicate glasses". *Contributions to Mineralogy and Petrology* 104(2), pages 142–162. DOI: 10.1007/bf00306439.

Simon, A. C. and E. M. Ripley (2011). "The Role of Magmatic Sulfur in the Formation of Ore Deposits". *Reviews in Mineralogy and Geochemistry* 73(1), pages 513–578. DOI: 10.2138/rmg.2011.73.16.

Smythe, D. J., B. J. Wood, and E. S. Kiseeva (2017). "The S content of silicate melts at sulfide saturation: New experiments and a model incorporating the effects of sulfide composition". *American Mineralogist* 102(4), pages 795–803. DOI: 10.2138/am-2017-5800ccby.

Soule, S., D. Nakata, D. Fornari, A. Fundis, M. Perfit, and M. Kurz (2012). "CO_2 variability in mid-ocean ridge basalts from syn-emplacement degassing: Constraints on eruption dynamics". *Earth and Planetary Science Letters* 327–328, pages 39–49. DOI: 10.1016/j.epsl.2012.01.034.

Spera, F. J. and S. C. Bergman (1980). "Carbon Dioxide in igneous petrogenesis: I: Aspects of the dissolution of CO_2 in silicate liquids". *Contributions to Mineralogy and Petrology* 74(1), pages 55–66. DOI: 10.1007/bf00375489.

Stanley, B. D., M. M. Hirschmann, and A. C. Withers (2014). "Solubility of COH volatiles in graphite-saturated martian basalts". *Geochimica et Cosmochimica Acta* 129, pages 54–76. DOI: 10.1016/j.gca.2013.12.013.

Stewart, C., D. E. Damby, C. J. Horwell, T. Elias, E. Ilyinskaya, I. TomaÅ¡ek, B. M. Longo, A. Schmidt, H. K. Carlsen, E. Mason, P. J. Baxter, S. Cronin, and C. Witham (2021). "Volcanic air pollution and human health: recent advances and future directions". *Bulletin of Volcanology* 84(1). DOI: 10.1007/s00445-021-01513-9.

Stolper, E. (1982a). "The speciation of water in silicate melts". *Geochimica et Cosmochimica Acta* 46(12), pages 2609–2620. DOI: 10.1016/0016-7037(82)90381-7.

– (1982b). "Water in silicate glasses: An infrared spectroscopic study". *Contributions to Mineralogy and Petrology* 81(1), pages 1–17. DOI: 10.1007/bf00371154.

Stolper, E., G. Fine, T. Johnson, and S. Newman (1987). "Solubility of carbon dioxide in albitic melt". *American Mineralogist* 72(11-12), pages 1071–1085.

Sun, C. and C.-T. A. Lee (2022). "Redox evolution of crystallizing magmas with C-H-O-S volatiles and its implications for atmospheric oxygenation". *Geochimica et Cosmochimica Acta* 338, pages 302–321. DOI: 10.1016/j.gca.2022.09.044.

Sun, C. and L. Yao (2024). "Redox equilibria of iron in low- to high-silica melts: A simple model and its applications to C-H-O-S degassing". *Earth and Planetary Science Letters* 638, page 118742. DOI: 10.1016/j.epsl.2024.118742.

Thibault, Y. and J. R. Holloway (1994). "Solubility of CO_2 in a Ca-rich leucitite: effects of pressure, temperature, and oxygen fugacity". *Contributions to Mineralogy and Petrology* 116(1–2), pages 216–224. DOI: 10.1007/bf00310701.

Wallace, P. J., V. S. Kamenetsky, and P. Cervantes (2015). "Melt inclusion CO_2 contents, pressures of olivine crystallization, and the problem of shrinkage bubbles". *American Mineralogist* 100(4), pages 787–794. DOI: 10.2138/am-2015-5029.

Wanless, V. D., A. M. Shaw, M. D. Behn, S. A. Soule, J. Escartín, and C. Hamelin (2015). "Magmatic plumbing at Lucky Strike volcano based on olivine-hosted melt inclusion compositions". *Geochemistry, Geophysics, Geosystems* 16(1), pages 126–147. DOI: 10.1002/2014gc005517.

Werner, C., D. J. Rasmussen, T. Plank, P. J. Kelly, C. Kern, T. Lopez, J. Gliss, J. A. Power, D. C. Roman, P. Izbekov, and J. Lyons (2020). "Linking Subsurface to Surface Using Gas Emission and Melt Inclusion Data at Mount Cleveland Volcano, Alaska". *Geochemistry, Geophysics, Geosystems* 21(7). DOI: 10.1029/2019gc008882.

Wetzel, D. T., M. J. Rutherford, S. D. Jacobsen, E. H. Hauri, and A. E. Saal (2013). "Degassing of reduced carbon from planetary basalts". *Proceedings of the National Academy of Sciences* 110(20), pages 8010–8013. DOI: 10.1073/pnas.1219266110.

Wieser, P. E. and M. Gleeson (2023). "PySulfSat: An open-source Python3 Tool for modeling sulfide and sulfate saturation". *Volcanica* 6(1), pages 107–127. DOI: 10.30909/vol.06.01.107127.

Wieser, P. E., K. Iacovino, S. Matthews, G. Moore, and C. M. Allison (2022a). "VESIcal: 2. A Critical Approach to Volatile Solubility Modeling Using an Open-Source Python3 Engine". *Earth and Space Science* 9(2). DOI: 10.1029/2021ea001932.

Wieser, P. E., H. Lamadrid, J. Maclennan, M. Edmonds, S. Matthews, K. Iacovino, F. E. Jenner, C. Gansecki, F. Trusdell, R. L. Lee, and E. Ilyinskaya (2021). "Reconstructing Magma Storage Depths for the 2018 Kīlauean Eruption From Melt Inclusion CO_2 Contents: The Importance of Vapor Bubbles". *Geochemistry, Geophysics, Geosystems* 22(2). DOI: 10.1029/2020gc009364.

Wieser, P. E., M. Petrelli, J. Lubbers, E. Wieser, S. Ozaydin, A. Kent, and C. Till (2022b). "Thermobar: An open-source Python3 tool for thermobarometry and hygrometry". *Volcanica* 5(2), pages 349–384. DOI: 10.30909/vol.05.02.349384.

Witham, F., J. Blundy, S. C. Kohn, P. Lesne, J. Dixon, S. V. Churakov, and R. Botcharnikov (2012). "SolEx: A model for mixed COHSCl-volatile solubilities and exsolved gas compositions in basalt". *Computers & Geosciences* 45, pages 87–97. DOI: 10.1016/j.cageo.2011.09.021.

Zajacz, Z. and A. Tsay (2019). "An accurate model to predict sulfur concentration at anhydrite saturation in silicate melts". *Geochimica et Cosmochimica Acta* 261, pages 288–304. DOI: 10.1016/j.gca.2019.07.007.

Zhang, H. L., E. Cottrell, P. A. Solheid, K. A. Kelley, and M. M. Hirschmann (2018). "Determination of $Fe^{3+}/\Sigma Fe$ of XANES basaltic glass standards by Mössbauer spectroscopy and its application to the oxidation state of iron in MORB". *Chemical Geology* 479, pages 166–175. DOI: 10.1016/j.chemgeo.2018.01.006.